number of apoptotic tumor cells (apoptotic index) measured in the control group was 6.2 ± 2.6. The MTD S-1 group did not show any significant difference (6.1 ± 4.9). However, the metronomic S-1 and vandetanib groups showed a significant increase in the apoptosis index (26.0 ± 5.4 and 18.4 ± 8.8, respectively, $P < .0001$). A significant increase in the tumor cell apoptosis index was also observed in the metronomic S-1 plus vandetanib group with 42 ± 3.5 ($P < .0001$).

Expression of VEGF and TSP-1 in Tumor Tissues

The results in Figure 6 show the expression of TSP-1 and VEGF in treated tumor tissues. The expression level of TSP-1 was significantly upregulated by approximately two- to three-fold in both the metronomic S-1 and the metronomic S-1 plus vandetanib treatment groups ($P < .05$ compared with the control group; Figure 6, *A* and *B*). With respect to expression levels of VEGF, there were no differences between the control and the MTD S-1 and metronomic S-1 groups (Figure 6, *C* and *D*). In contrast, the vandetanib and the metronomic S-1 plus vandetanib groups showed significantly upregulated the VEGF expression compared with the control group ($P < .05$; Figure 6, *C* and *D*). There was a significant difference between the vandetanib monotherapy group and the metronomic S-1 plus vandetanib treatment group ($P = .045$).

Discussion

Our results add to an expanding body of literature reporting the therapeutic benefit of metronomic chemotherapy, especially when it is combined concurrently with a targeted antiangiogenic drug [5,12,13]. Moreover, to our knowledge, this is the first preclinical report of using S-1 in a metronomic dosing and administration schedule for HCC preclinical model. Also noteworthy is that we undertook a comparative

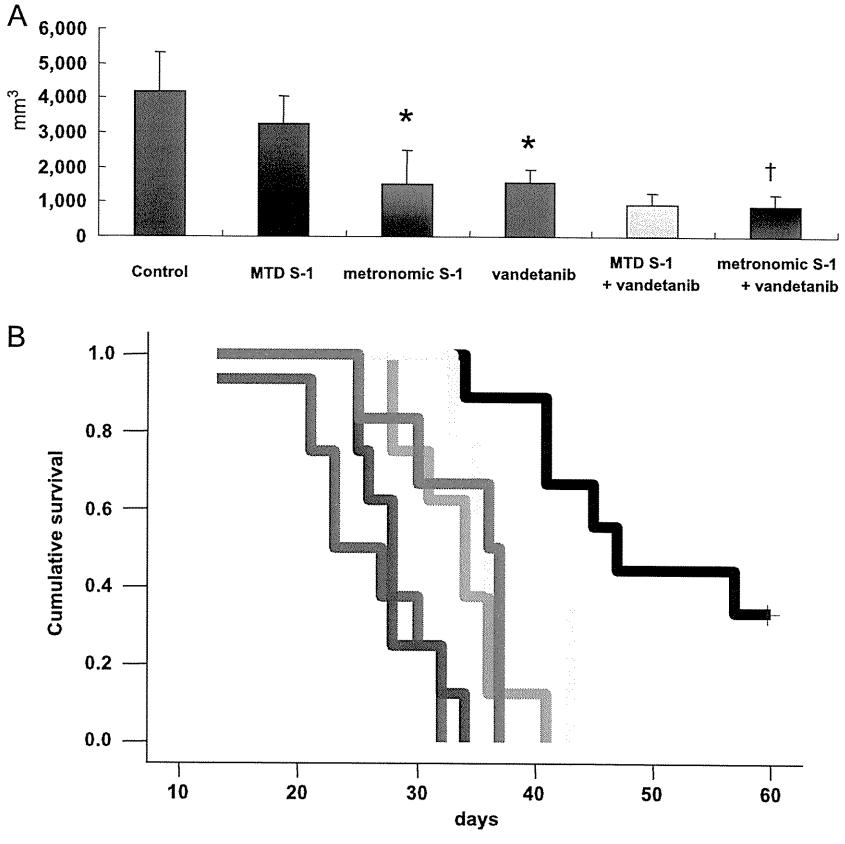

Figure 4. Assessment of therapeutic effects in KYN-2 liver transplant model. Tumor-bearing nude mice were treated in the following six groups: 1) HPMC as the control group (blue); 2) MTD S-1: 15 mg/kg per day for 1 week, followed by 1 week break period (purple); 3) metronomic S-1: 5 mg/kg per day for 2 weeks without break period (green); 4) vandetanib 25 mg/kg per day for 2 weeks (red); 5) MTD S-1 with vandetanib (yellow); or 6) metronomic S-1 with vandetanib (black). (A) Inhibition of tumor growth for KYN-2 liver transplant model. All treatments were performed 4 weeks in total. There was no significant difference between the control and the MTD S-1 groups. The metronomic S-1 group contributed to obvious inhibitory effect of tumor growth (*$P < .05$ compared with the control and the MTD S-1 groups). The metronomic S-1 with vandetanib treatment group showed the greatest inhibitory effect of tumor growth among all the groups (†$P < .001$). (B) Survival of mice treated with MTD S-1 or metronomic S-1 and in combination with vandetanib ($n = 10$ per group). Treatment was continued until mice were moribund, and days of life were recorded. Survival data were compared for significance with the log-rank test. MTD S-1 did not prolong survival compared with the control group. In contrast, metronomic S-1 prolonged survival compared with the control and MTD S-1 groups. The metronomic S-1 with vandetanib group provided the most effective therapy with longest survival times among all the groups ($P < .001$).

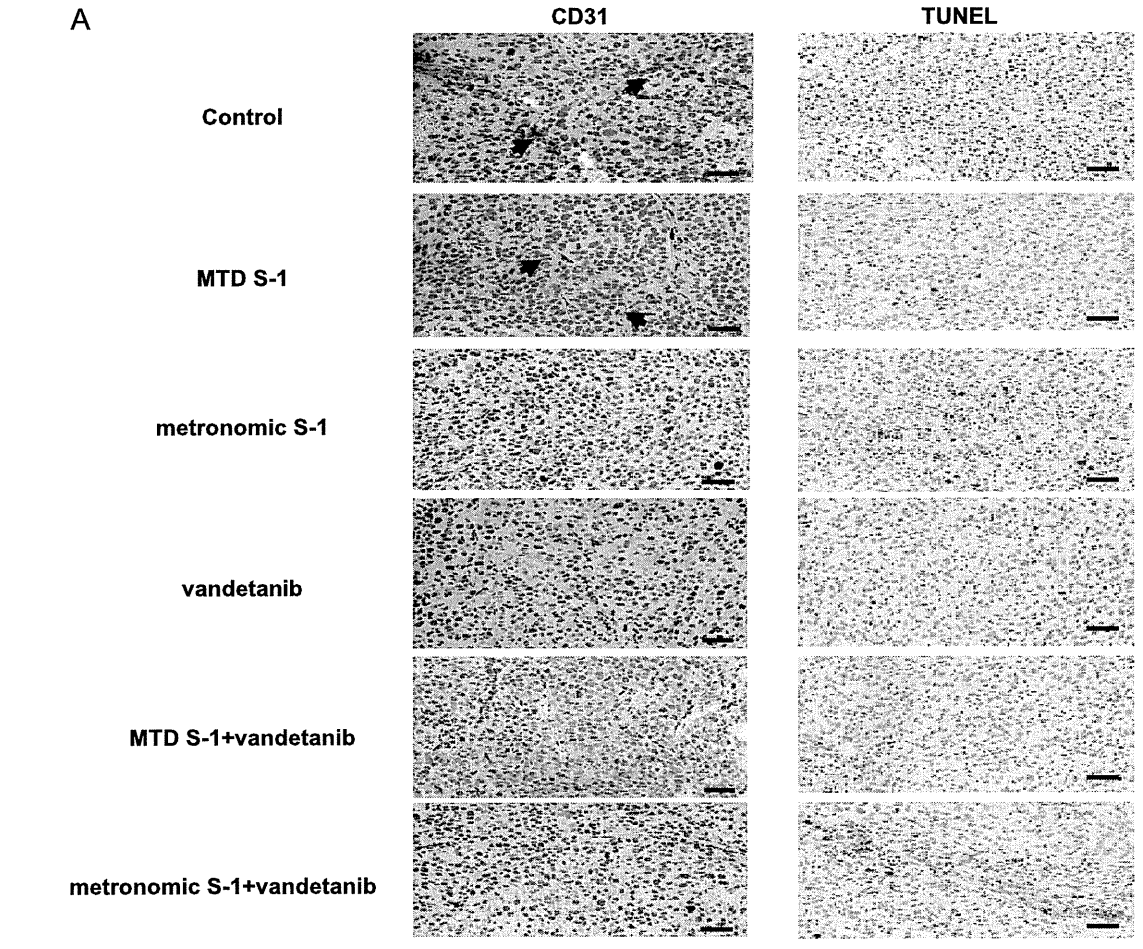
A
CD31
TUNEL
Control
MTD S-1
metronomic S-1
vandetanib
MTD S-1+vandetanib
metronomic S-1+vandetanib

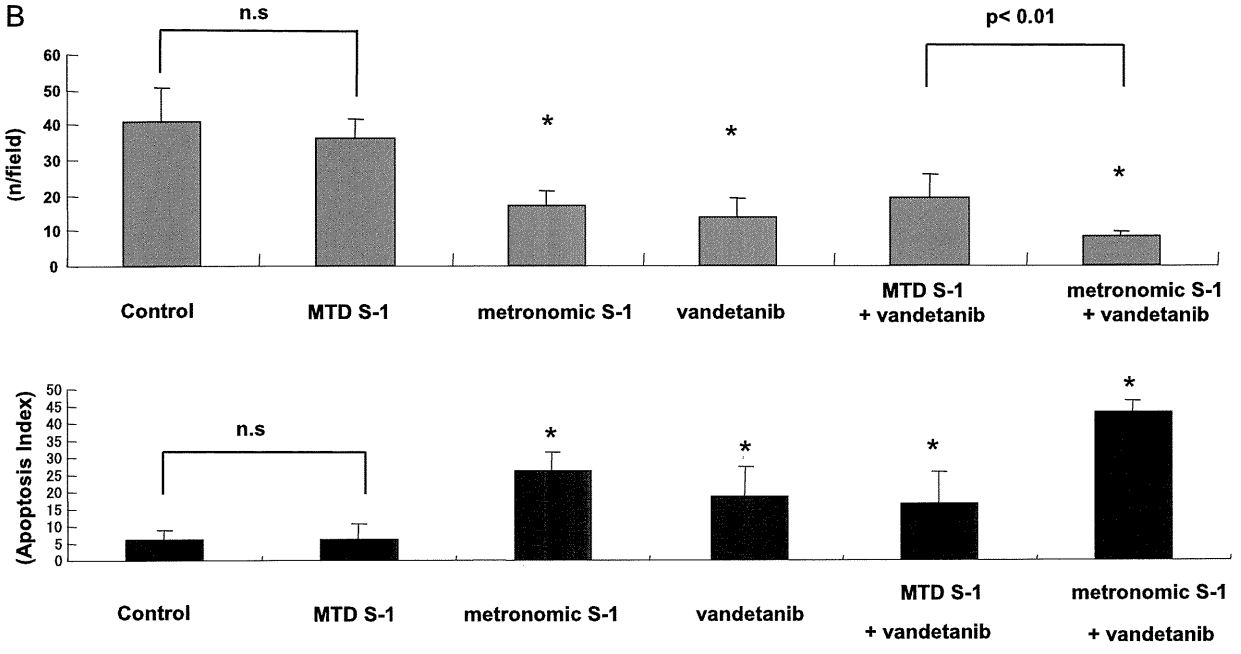
B
n.s
p< 0.01
(n/field)
60
50
40
30
20
10
0
*
Control
MTD S-1
metronomic S-1
vandetanib
MTD S-1
+ vandetanib
metronomic S-1
+ vandetanib
(Apoptosis Index)
50
45
40
35
30
25
20
15
10
5
0
n.s
Control
MTD S-1
metronomic S-1
vandetanib
MTD S-1
+ vandetanib
metronomic S-1
+ vandetanib

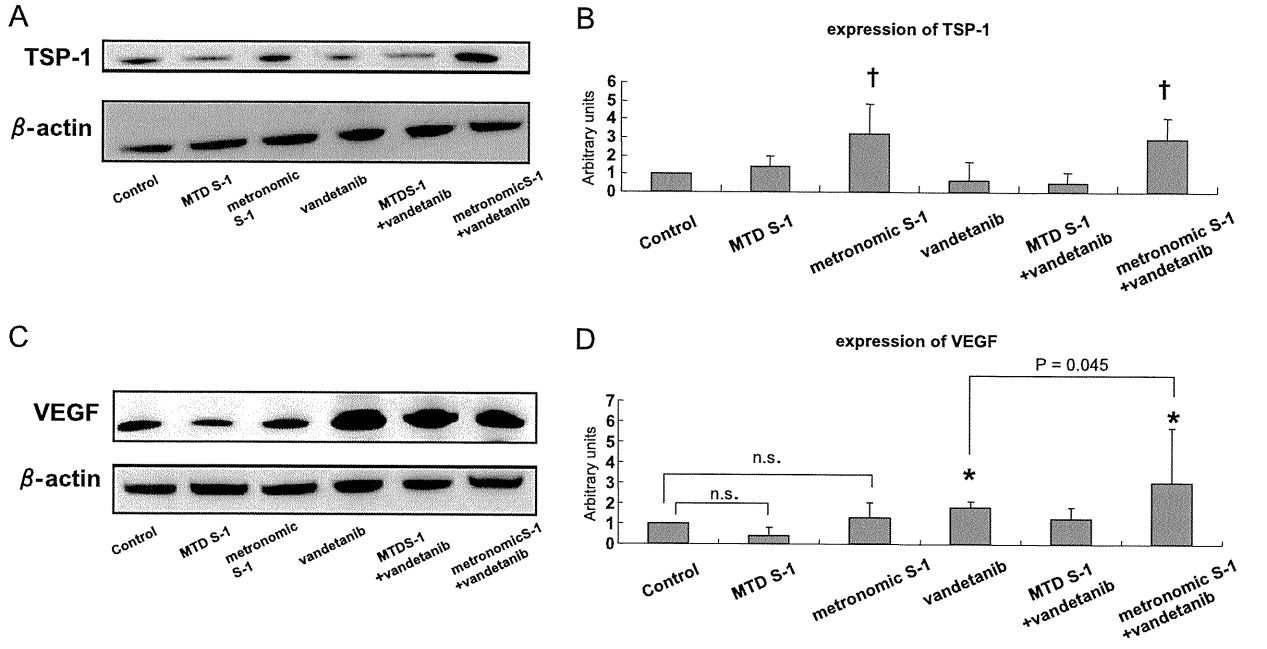

Figure 6. Western blot analysis of TSP-1 and VEGF. The band intensities of both TSP-1 and VEGF in treatment groups were measured and calibrated with each protein in control group and β-actin. (A and B) The metronomic S-1 and metronomic S-1 with vandetanib groups showed strongly upregulated the expression of TSP-1 ($^{\dagger}P < .001$ compared with the control group). (C and D) The expression of tumor VEGF was increased by the vandetanib and the metronomic S-1 with vandetanib groups. There were no differences between the control and the MTD S-1, metronomic S-1 group ($^{*}P < .05$ compared with the control group). There was a significant difference between the vandetanib and metronomic S-1 with vandetanib group ($P = .045$).

analysis of the effects of S-1 given in a more conventional MTD schedule with metronomic S-1, and our results consistently showed the metronomic dosing/schedule was superior to the MTD protocol, both in terms of increased antitumor efficacy and reduced toxicity. Importantly, in this regard, the metronomic protocol we used involved a cumulative dose over time that was 30% less than the corresponding MTD protocol. Below we discuss a number of different aspects of our results and some of the translational/clinical implications.

Antiangiogenic Effects Mediated by Metronomic S-1 Chemotherapy

Previous studies during the last decade have indicated that metronomic chemotherapy regimens using cytotoxic agents inhibit tumor growth by various mechanisms, namely, antiangiogenic effects, direct tumor cell targeting effects, or anticancer immune responses [4,19, 20]. Our results with metronomic S-1 would seem to confirm the antiangiogenic effect findings. First, we found that exposure of 5-FU in a metronomic-type protocol *in vitro* brought about a greater antiproliferative effect at distinctly low concentrations not only of 5-FU on two different tumor cell lines but also, especially, HUVECs, compared with an MTD-like exposure. This is similar to the results of other studies such as that of Bocci et al. [16] using paclitaxel or the active metabolite of cyclophosphamide. Second, we found reduced MVD and increased number of apoptotic tumor cells in mice treated with the metronomic S-1 schedule but not the MTD protocol. Third, we observed an increased expression of TSP-1, which has been reported previously using other cytotoxic drugs administered in a metronomic fashion *in vivo*, including cyclophosphamide [21]. Fourth, we noted that a tumor cell line (KYN-2) that is intrinsically resistant *in vitro* to high concentrations of 5-FU—the major metabolite of S-1—nevertheless responds to metronomic S-1 *in vivo* but not to MTD S-1, suggesting that a target other than the tumor cell population *per se* is likely involved in the *in vivo*

Figure 5. MVD and apoptosis in tumors tissues. The sections of tumors from the KYN-2 liver transplant model were stained by anti-CD31 antibody and Terminal deoxynucleotidyl transferase (TdT)–mediated dUTP nick-end labeling (TUNEL). Original magnification, ×200. The density of CD31-positive vessels (arrow) and TUNEL in a tumor field are represented as mean ± SD ($n = 30$ per group). (A) Representative sections for each treatment are shown. Bar, 10 μm. (B) There was no significant difference in MVD between the control and the MTD S-1 groups. Tumor vessel numbers were reduced by metronomic S-1. The metronomic S-1 with vandetanib group showed the most inhibitory effect of tumor vessel count among all the groups ($^{*}P < .001$ compared with the control group and the MTD S-1 group). The MTD S-1 group did not show any significant difference in the number of tumor cell apoptosis index (6.1 ± 4.9). However, the metronomic S-1 and vandetanib groups significantly increased in the number of apoptosis index, respectively (26.0 ± 5.4 and 18.4 ± 8.8, $P < .0001$). A significant increase of tumor cell apoptosis index was also observed in the metronomic S-1 with vandetanib group with 42 ± 3.5 ($P < .0001$).

antitumor activity that was observed using metronomic S-1. Fifth, O'Reilly et al. [22] have reported that the antiangiogenic effect mediated by endogenous antiangiogenic factors induces increased apoptosis of tumor cells, likely a secondary effect due to decreased MVD, whereas proliferation of tumor cells was not affected. Similarly, tumor apoptotic cell numbers were increased, whereas proliferation of tumor cells was not inhibited by metronomic S-1 chemotherapy in our study. On the basis of all of the aforementioned data and information, the antitumor effect of metronomic S-1 chemotherapy was likely to be mainly through antiangiogenesis mediated by inhibiting the proliferation of endothelial cells and inducing the expression of TSP-1, although some additional mechanisms cannot be entirely excluded. The mechanism of antiangiogenesis of metronomic S-1 chemotherapy is thought to be quite different from that of vandetanib. Inhibiting VEGFR by vandetanib resulted in increased VEGF production in tumor tissues, paradoxically, whereas metronomic S-1 chemotherapy did not increase VEGF production. Ebos et al. [23] reported that this difference of production of VEGFs influenced to achieving malignant potential of cancer cells. Also, at this point, metronomic chemotherapy is thought to be a promising strategy of long-term treatment of cancer.

Translational/Clinical Implications of the Metronomic S-1 + Vandetanib Preclinical Results

There are several potentially important implications of our results with respect to how they might conceivably be exploited for the future treatment and management of HCC patients. It is well known that there are no effective chemotherapy regimens for the treatment of advanced HCC using conventional chemotherapy regimens. One reason for this is the frequent underlying liver dysfunction [2]. As a consequence, using MTD given in conventional schedules is often contraindicated because of possible excessive toxicity. However, chemotherapy drugs given in a metronomic, less toxic fashion may be an alternative strategy to circumvent this problem. In this regard, there is conflicting evidence regarding the clinical benefit of metronomic UFT, another 5-FU prodrug, at least in the postoperative adjuvant use for HCC [24]. However, some aspects regarding the negative clinical findings should be taken into consideration. One is the dosing. The daily dose used in the aforementioned adjuvant study was less than the dose used for a positive phase 3 adjuvant UFT clinical trial for non–small cell lung cancer patients [9]. The second is the benefit that might be gained by using an antiangiogenic drug in combination with metronomic UFT. For example, a recent report by Tang et al. showed that neither metronomic UFT nor antiangiogenic drug therapy alone had overt antitumor activity in a model of locally advanced HCC, whereas these drugs when combined showed significant antitumor activity [25]. Also, in our study, combining with vandetanib resulted in enhanced antitumor effects for S-1 chemotherapy; nevertheless, MTD S-1 monotherapy did not show any effective antitumor effects. VEGFR is related to chemoresistance for tumor endothelial cells through surviving [26]. Inhibiting VEGFR by vandetanib might have contributed to enhanced chemosensitivity for tumor endothelial cells. And EGFR is associated with resistance to 5-FU [15]. Inhibiting EGFR by vandetanib might have enhanced chemosensitivity to 5-FU. In addition, it is notable in our study that not only the combination with vandetanib but also metronomic S-1 monotherapy showed significant antitumor effects. Because S-1 may be superior to UFT in antitumor effect by virtue of its biochemical modulators [7], S-1 might be an even more suitable agent for metronomic chemotherapy.

In summary, we have demonstrated preclinically that metronomic S-1 chemotherapy showed effective therapeutic outcomes without overt toxicity for treatment of HCC, mainly by suppressing tumor angiogenesis, and the activity of which is amplified by concurrent combination with vandetanib. Metronomic S-1 and the concurrent combination treatment with an antiangiogenic agent might be a promising treatment strategy for HCC.

References

[1] Parkin D, Bray F, Ferlay J, and Pisani P (2001). Estimating the world cancer burden Globocan 2000. *Int J Cancer* **94**, 153–156.

[2] Llovet J, Di Bisceglie A, Bruix J, Kramer B, Lencioni R, Zhu A, Sherman M, Schwartz M, Lotze M, Talwalkar J, et al. (2008). Design and endpoints of clinical trials in hepatocellular carcinoma. *J Natl Cancer Inst* **100**, 698–711.

[3] Kim JJ and Tannock IF (2005). Repopulation of cancer cells during therapy: an important cause of treatment failure. *Nat Rev Cancer* **5**(7), 516–525.

[4] Kerbel R and Kamen B (2004). The anti-angiogenic basis of metronomic chemotherapy. *Nat Rev Cancer* **4**, 423–436.

[5] Munoz R, Man S, Shaked Y, Lee C, Wong J, Francia G, and Kerbel R (2006). Highly efficacious nontoxic preclinical treatment for advanced metastatic breast cancer using combination oral UFT-cyclophosphamide metronomic chemotherapy. *Cancer Res* **66**, 3386–3391.

[6] Man S, Bocci G, Francia G, Green S, Jothy S, Hanahan D, Bohlen P, Hicklin D, Bergers G, and Kerbel R (2002). Antitumor effects in mice of low-dose (metronomic) cyclophosphamide administered continuously through the drinking water. *Cancer Res* **62**, 2731–2735.

[7] Fukushima M, Satake H, Uchida J, Shimamoto Y, Kato T, Takechi T, Okabe H, Fujioka A, Nakano K, Ohshimo H, et al. (1998). Preclinical antitumor efficacy of S-1: a new oral formulation of 5-fluorouracil on human tumor xenografts. *Int J Oncol* **13**, 693–698.

[8] Koizumi W, Narahara H, Hara T, Takagane A, Akiya T, Takagi M, Miyashita K, Nishizaki T, Kobayashi O, Takiyama W, et al. (2008). S-1 plus cisplatin *versus* S-1 alone for first-line treatment of advanced gastric cancer (SPIRITS trial): a phase III trial. *Lancet Oncol* **9**, 215–221.

[9] Kato H, Ichinose Y, Ohta M, Hata E, Tsubota N, Tada H, Watanabe Y, Wada H, Tsuboi M, and Hamajima N (2004). A randomized trial of adjuvant chemotherapy with uracil-tegafur for adenocarcinoma of the lung. *N Engl J Med* **350**, 1713–1721.

[10] Watanabe T, Sano M, Takashima S, Kitaya T, Tokuda Y, Yoshimoto M, Kohno N, Nakagami K, Iwata H, Shimozuma K, et al. (2009). Oral uracil and tegafur compared with classic cyclophosphamide, methotrexate, fluorouracil as postoperative chemotherapy in patients with node-negative, high-risk breast cancer: National Surgical Adjuvant Study for Breast Cancer 01 Trial. *J Clin Oncol* **27**, 1368–1374.

[11] Llovet J, Ricci S, Mazzaferro V, Hilgard P, Gane E, Blanc J, de Oliveira A, Santoro A, Raoul J, Forner A, et al. (2008). Sorafenib in advanced hepatocellular carcinoma. *N Engl J Med* **359**, 378–390.

[12] Klement G, Baruchel S, Rak J, Man S, Clark K, Hicklin D, Bohlen P, and Kerbel R (2000). Continuous low-dose therapy with vinblastine and VEGF receptor-2 antibody induces sustained tumor regression without overt toxicity. *J Clin Invest* **105**, R15–R24.

[13] Pietras K and Hanahan D (2005). A multitargeted, metronomic, and maximum-tolerated dose "chemo-switch" regimen is antiangiogenic, producing objective responses and survival benefit in a mouse model of cancer. *J Clin Oncol* **23**, 939–952.

[14] Wedge S, Ogilvie D, Dukes M, Kendrew J, Chester R, Jackson J, Boffey S, Valentine P, Curwen J, Musgrove H, et al. (2002). ZD6474 inhibits vascular endothelial growth factor signaling, angiogenesis, and tumor growth following oral administration. *Cancer Res* **62**, 4645–4655.

[15] Wang H, Jiang H, Zhou M, Xu Z, Liu S, Shi B, Yao X, Yao M, Gu J, and Li Z (2009). Epidermal growth factor receptor VIII enhances tumorigenicity and resistance to 5-fluorouracil in human hepatocellular carcinoma. *Cancer Lett* **279**, 30–38.

[16] Bocci G, Francia G, Man S, Lawler J, and Kerbel R (2003). Thrombospondin 1, a mediator of the antiangiogenic effects of low-dose metronomic chemotherapy. *Proc Natl Acad Sci USA* **100**, 12917–12922.

[17] Kamat A, Kim T, Landen CJ, Lu C, Han L, Lin Y, Merritt W, Thaker P, Gershenson D, Bischoff F, et al. (2007). Metronomic chemotherapy enhances the efficacy of antivascular therapy in ovarian cancer. *Cancer Res* **67**, 281–288.

[18] Zhang X and Lawler J (2007). Thrombospondin-based antiangiogenic therapy. *Microvasc Res* **74**, 90–99.

[19] Ghiringhelli F, Menard C, Puig P, Ladoire S, Roux S, Martin F, Solary E, Le Cesne A, Zitvogel L, and Chauffert B (2007). Metronomic cyclophosphamide regimen selectively depletes $CD4^+CD25^+$ regulatory T cells and restores T and NK effector functions in end stage cancer patients. *Cancer Immunol Immunother* **56**, 641–648.

[20] Pasquier E, Kavallaris M, and André N (2010). Metronomic chemotherapy: new rationale for new directions. *Nat Rev Clin Oncol* **7**, 455–465.

[21] Bocci G, Nicolaou K, and Kerbel R (2002). Protracted low-dose effects on human endothelial cell proliferation and survival *in vitro* reveal a selective antiangiogenic window for various chemotherapeutic drugs. *Cancer Res* **62**, 6938–6943.

[22] O'Reilly M, Boehm T, Shing Y, Fukai N, Vasios G, Lane W, Flynn E, Birkhead J, Olsen B, and Folkman J (1997). Endostatin: an endogenous inhibitor of angiogenesis and tumor growth. *Cell* **88**, 277–285.

[23] Ebos J, Lee C, Munoz W, Bjamason G, Christensen J, and Kerbel R (2009). Accelerated metastasis after short-term treatment with a potent inhibitor of tumor angiogenesis. *Cell Press* **15**, 232–239.

[24] Hasegawa K, Takayama T, Ijichi M, Matsuyama Y, Imamura H, Sano K, Sugawara Y, Kokudo N, and Makuuchi M (2006). Uracil-tegafur as an adjuvant for hepatocellular carcinoma: a randomized trial. *Hepatology* **44**, 891–895.

[25] Tang T, Man S, Lee C, Xu P, and Kerbel R (2010). Impact of metronomic UFT/cyclophosphamide chemotherapy and antiangiogenic drug assessed in a new preclinical model of locally advanced orthotopic hepatocellular carcinoma. *Neoplasia* **12**, 264–274.

[26] Tran J, Master Z, Yu J, Rak J, Dumont D, and Kerbel R (2002). A role for survivin in chemoresistance of endothelial cells mediated by VEGF. *Proc Natl Acad Sci USA* **99**, 4349–4354.

Periostin, a matrix protein, has potential as a novel serodiagnostic marker for cholangiocarcinoma

KIMINORI FUJIMOTO[1,2], TAKUMI KAWAGUCHI[3], OSAMU NAKASHIMA[4], JUNYA ONO[6], SHOICHIRO OHTA[7], ATSUSHI KAWAGUCHI[5], TATSUYUKI TONAN[1], KOICHI OHSHIMA[4], HIROHISA YANO[4], NAOFUMI HAYABUCHI[1], KENJI IZUHARA[8] and MICHIO SATA[3]

[1]Department of Radiology, Kurume University School of Medicine and [2]Center for Diagnostic Imaging, Kurume University Hospital, 67 Asahi-machi, Kurume, 830-0011; Departments of [3]Digestive Disease Information and Research and Department of Medicine, and [4]Pathology, [5]Biostatistics Center, Kurume University School of Medicine, Kurume; [6]Shino-Test Corporation, Sagamihara; Departments of [7]Laboratory Medicine and [8]Biomolecular Sciences, Saga Medical School, Saga, Japan

Received December 10, 2010; Accepted January 30, 2011

DOI: 10.3892/or.2011.1194

Abstract. Differentiating intrahepatic cholangiocarcinoma (CCA) from other hepatic malignancies is crucial in deciding on treatment modalities and predicting clinical outcomes in patients. Periostin is a secreted protein from stromal cells and regulates the development of cancer cells through interaction with the extracellular matrix. Given that proliferation of fibrous stromal cells is a pathological feature of CCA, we examined the potential use of periostin as a serodiagnostic marker for this disease. Our study enrolled a total of 79 patients including liver cirrhosis (n=26), hepatocellular carcinoma (HCC, n=24), CCA (n=8), other hepatic malignancies (n=13) and histologically normal livers (normal control, n=8). Periostin expression was evaluated using immunohistochemistry and serum periostin level was determined via enzyme-linked immunoassay. The diagnostic performance of serum periostin levels for distinguishing CCA patients from others was also assessed. Strong expression of periostin was noted only in the fibrous stroma of CCA tissue. Serum periostin levels (median) were significantly higher in patients with CCA (513 ng/ml) compared to those patients with normal liver, liver cirrhosis, HCC and other malignancies (120, 146, 155, 213 ng/ml, respectively, all $P<0.05$). The area under receiver operating characteristics curve of serum periostin level was 0.94 [95% confidence interval (CI), 0.85-1.00, $P<0.001$]. With optimal cut-off value of 302 ng/ml, diagnostic performances for CCA were as follows: sensitivity, 0.88 (95% CI, 0.47-0.99); specificity, 0.92 (0.83-0.96); accuracy, 0.91 (0.83-0.96); positive predictive value, 0.54 (0.25-0.81); negative predictive value, 0.98 (0.92-0.99); positive-likelihood ratio, 10.4 (4.8-13.4); and negative-likelihood ratio, 0.13 (0.03-0.49). We demonstrated increased expression of periostin in the stroma of CCA tissue. Serum periostin levels were significantly elevated in patients with CCA and enable distinction between CCA and other hepatic malignancies.

Correspondence to: Dr Kiminori Fujimoto, Department of Radiology, Kurume University School of Medicine and Center for Diagnostic Imaging, Kurume University Hospital, 67 Asahi-machi, Kurume 830-0011, Japan
E-mail: kimichan@med.kurume-u.ac.jp

Abbreviations: CCA, cholangiocarcinoma; HCC, hepatocellular carcinoma; CA19-9, carbohydrate antigen 19-9; CEA, carcinoembryonic antigen; AFP, α-fetoprotein; phosphate-buffered saline; ELISA, enzyme-linked immunosorbent assay; PBS, phosphate-buffered saline; ROC, receiver operating characteristics; PPV, positive predictive value; NPV, negative predictive value; LR, likelihood ratio; AUC, the area under the ROC curve; TGF-β, transforming growth factor β

Key words: periostin, cholangiocarcinoma, tumor marker, enzyme-linked immunosorbent assay, hepatocellular carcinoma

Introduction

Periostin is a newly emerged extracellular matrix protein belonging to the fasciclin family (1-3). Periostin enhances collagen fibrillogenesis by binds to collagen I, fibronectin, and tenascin-C (4-6) and by activating lysyl oxidase, a catalytic enzyme for cross-linking of collagen (7). Furthermore, periostin acts as a matricellular protein by binding to several integrin molecules, $\alpha_v\beta_1/\beta_3$, on cell surface, involved in tissue development and carcinogenesis (1,2,8). In malignant cells, periostin activates phosphatidylinositol 3-kinase and Akt pathways via integrin molecules, which are important for growth, migration, and epithelial-mesenchymal transition of the cells (9-11). Malignant cells themselves or stromal cells adjacent to malignant cells are sources of periostin (8).

Recent studies have reported that increased expression of periostin in some cancers with fibrous stromal cells including non-small cell lung carcinoma and breast cancer (12-14). The pathological feature of intrahepatic cholangiocarcinoma (CCA), but not hepatocellular carcinoma (HCC), is abundant in fibrous stromal cells (15), and that raised a possibility that expression of periostin is differently regulated in CCA and HCC. Indeed, it has been very recently shown that CCA-associated fibroblasts or CCA-containing tissues strongly

Table I. Patient characteristics.

	Reference value	Normal liver	Liver cirrhosis	HCC	Other hepatic malignancies	CCA	P-values[a]
Number	N/A	8	26	24	13	8	
Age (years)	N/A	56 (36-65)	59 (51-65)	70 (64-75)	61 (55-72)	59 (50-73)	0.090
Gender (male/female)	N/A	2/6	11/15	19/5	12/1	4/4	0.020
AFP (ng/ml)	<8.7	N/A	N/A	20 (4.1-173)	11.6 (5.5-76)	4.9 (3.4-5.9)	0.057
CEA (ng/ml)	<5.0	N/A	N/A	3.2 (2.1-3.4)[b]	3.3 (2.3-4.3)	3.8 (3.3-6.1)[b]	0.028[b]
CA19-9 (U/ml)	<37.0	N/A	N/A	47 (32-79)	47 (26-53)	96 (27-1323)	0.354
Periostin (ng/ml)	Unknown	120 (86-194)	146 (113-194)	155 (110-213)	213 (154-283)	513 (315-897)	<0.0001[c]

Data are expressed as median (25th to 75th percentile of interquartile range) or number of patients. HCC, hepatocellular carcinoma; CCA, cholangiocarcinoma; N/A, not-applicable; AFP, α-fetoprotein; CEA, carcinoembryonic antigen; CA19-9, carbohydrate antigen 19-9. [a]P-values are calculated using the Kruskal-Wallis test and Fisher's exact test. [b]Multiple pairwaise comparisons revealed that serum CEA level in the CCA group was significantly higher than that in HCC group (Bonferroni correction, P=0.024). [c]For serum periostin level, see Fig. 3 and description.

express periostin compared to non-tumorigenic liver fibroblasts or liver tissues containing HCC (16,17). Furthermore, an *in vitro* study found that periostin enhanced cell proliferation and invasion. CCA is one of the most devastating malignancies and differentiating CCA from HCC is crucial in deciding treatment modalities and predicting clinical outcomes, and patient counseling (18-21). Periostin is a secretory protein (11,22); however, it remains unclear whether expression of periostin in CCA tissues reflects serum level of periostin and whether measurement of serum level of periostin can be applied to differential diagnosis between CCA and HCC.

The aims of this study were to examine the tissue expression of periostin in CCA and the efficacy of periostin as a serodiagnostic marker for CCA.

Patients and methods

Patients. We retrospectively enrolled a total of 79 patients with liver cirrhosis (n=26), HCC (n=24), CCA (n=8), other hepatic malignancies (n=13), including combined type of HCC (n=7), scirrhous type of HCC (n=3) and HCC with sarcomatous change (n=3), or histologically normal livers obtained from hepatic resection or liver diagnostic biopsy for benign liver lesions (n=8), such as focal nodular hyperplasia or angiomyolipoma. All of the patients were hospitalized for diagnostic liver biopsy or radical hepatic resection for liver tumor. All of the diagnoses were based on clinical, serological, imaging and histological evidence and characteristics of enrolled patients are shown in Table I. The study protocol conformed to the ethical guidelines of the Declaration of Helsinki 2008 (23) as reflected in prior approval by the Ethics Committee of our institution. All patients gave the written informed consent.

Serum tumor markers. Venous blood samples were taken in the morning after a 12-h overnight fast. Serum α-fetoprotein (AFP), carcinoembryonic antigen (CEA), and CA19-9 levels were measured in all patients with malignant neoplasm (n=45) by using standard clinical methods (Department of Clinical Laboratory, Kurume University Hospital).

Histological diagnosis. For each patient, a liver specimen was fixed in 10% formalin buffer and stained with hematoxylin-eosin. All of histological diagnoses were performed by two experienced pathologist who were unaware of the patients' clinical and laboratory data.

Establishment of anti-periostin monoclonal and polyclonal antibodies (Abs). We newly established anti-periostin mAbs as previously reported (6). Briefly, 6-10-week-old Crj:Wistar rats (Charles River Japan, Inc., Kanagawa, Japan) were injected in footpads two or more times with 20 μg of recombinant human periostin emulsified in TiterMax Gold adjuvant (TiterMax USA, Norcross, GA). Three days after the last injection, lymphocytes from popliteal, inguinal and iliac lymph nodes were fused with a Sp2/O myeloma cell line. Rat anti-periostin mAbs were purified from culture supernatant of the hybridomas using a protein G affinity chromatography column. Specific pathogen-free rabbits were immunized with recombinant human periostin, and antiserum was obtained. Purified rabbit anti-human periostin polyclonal Ab was generated from the antiserum as previously reported (6).

Immunohistochemistry. Immunohistochemical analysis was performed as previously described (6,24-27). Paraffin-embedded liver sections were deparaffinized and were washed three times for 5 min each in phosphate-buffered saline (PBS) (pH 7.4, 130 mmol/l NaCl, 2 mmol/l NaH_2PO_4, and 7 mmol/l Na_2HPO_4) and then blocked with 10% skim milk in PBS for 30 min. Sections were incubated overnight at 4˚C with the rat anti-human periostin mAbs (clone no. SS19B or SS5D) diluted 1:100 in PBS. After several washes with PBS, the sections were incubated with the secondary antibodies, biotin-labeled goat anti-rat IgG diluted 1:100 in PBS at room temperature for 1 h. Subsequently, the sections were washed with PBS and Positive reactivity was identified using a Vectastain ABC kit (Vector Laboratories, Burlingame, CA) and developed with 3,3'-diaminobenzidine (Dako, Kyoto, Japan).

Establishment of enzyme-linked immunosorbent assay (ELISA). Serum were obtained before diagnosis or treatment

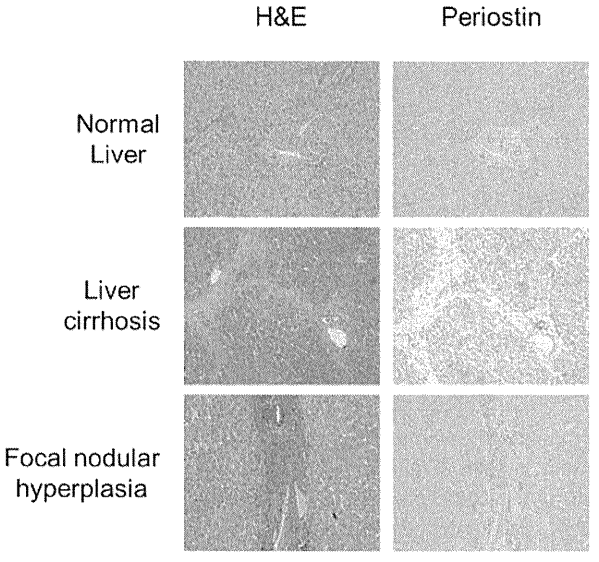

Figure 1. Immunostaining for periostin in non-malignant liver tissue. Sections from normal liver, liver cirrhosis, and focal nodular hyperplasia were immunostained with anti-periostin antibodies. Expression of periostin was visualized by 3,3'-diaminobenzidine (brown). Original magnification, x400.

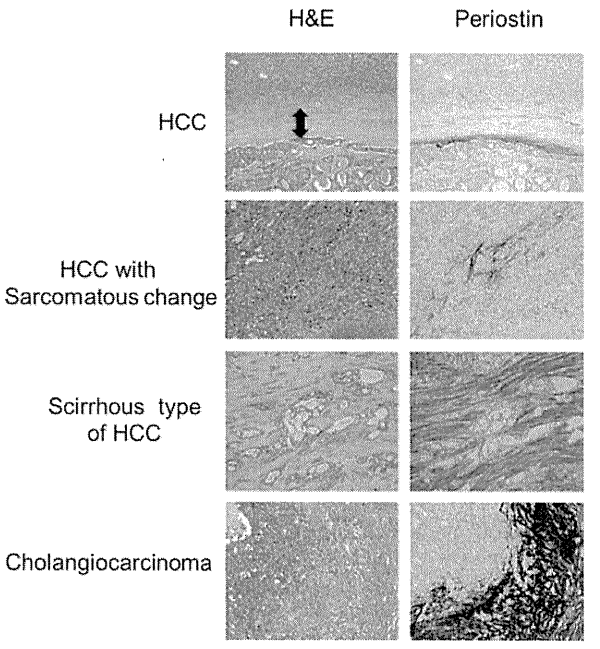

Figure 2. Immunostaining for periostin in hepatic malignant tissue. Sections from hepatocellular carcinoma (HCC), HCC with sarcomatous change, scirrhous type of HCC, and cholangiocarcinoma were immunostained with anti-periostin antibodies. Expression of periostin was visualized by 3,3'-diaminobenzidine (brown). Original magnification, x400. Arrow in left upper panel indicates capsule of HCC.

of hepatic malignancies and then stored at -80˚C until ELISA assay. We newly established a human periostin ELISA assay. Two rat anti-human periostin mAbs (clone no. SS16A and SS17B) were used to establish a sandwich ELISA assay. The SS16A mAb (2 μg/ml) was incubated overnight at 25˚C on ELISA plates (Loose MaxiSorp® Nunc-Immuno® Modules, Thermo Fisher Scientific, Rochester, NY). The ELISA plates were blocked by blocking buffer (0.5% casein, in TBS, pH 8.0) overnight at 4˚C and then washed three times with washing buffer (0.05% Tween-20 in PBS). The ELISA plates were incubated with diluted samples (1/6,000) or recombinant periostin standards for 18 h at 25˚C, followed by washing five times. Biotin-labeled SS17B mAb (5 μg/ml) was added followed by incubation for 90 min at 25˚C. After washing five times, diluted peroxidase-labeled streptavidin (1/15,000) (Strerospecific Detection Technologies) was added to the plates, which were then incubated for 1 h at 25˚C. After the ELISA plates were washed 5 times, reaction solution (0.8 mM 3,3',5,5'-Tetramethylbenzidine, 2.5 mM H_2O_2) was added, followed by incubation for 10 min at 25˚C and then the reaction was stopped by adding the stop solution (0.7 N HCl). The values were calculated by subtracting the absorbance at 550 nm (secondary wavelength) from the absorbance at 450 nm (primary wavelength) measured by a microplate reader (Bio-Rad Laboratories, Tokyo, Japan). Periostin concentrations in the serum were calculated simultaneously using the recombinant periostin proteins. We performed the ELISA assay on duplicated samples.

Statistical analysis. All continuous data were expressed as median and the 25th to the 75th percentile of the interquartile range.

The Kruskal-Wallis test was used to determine significance of intergroup differences of the serum periostin levels. In case of statistical significance, multiple pairwise comparisons were conducted with the Mann-Whitney U test with Bonferroni correction.

To test if serum periostin level can distinguish CCA group from other groups, bivariate logistic regression analysis was performed with serum periostin level as a covariate and each group and other group (dummy variables) as dependent variables. Receiver operating characteristic (ROC) analysis was used to determine the cut-off value of serum periostin levels for distinguishing CCA patients from others as previously described (28). The significance for the cut-off value of serum periostin was evaluated by sensitivity, specificity, accuracy, positive predictive value (PPV), negative predictive value (NPV), and likelihood ratio (LR). Finally, among hepatic malignant neoplasms (n=45) serum levels of tumor markers including AFP, CEA, CA19-9 and periostin for distinguishing CCA from other malignancies were reevaluated with ROC analysis.

All analyses were performed using SPSS statistical software (version 12.0J; SPSS, Inc., Chicago, IL) and $P<0.05$ was considered statistically significant.

Results

Immunohistochemistry for periostin. Although slight expression of periostin was seen in bile duct cells, no expression of periostin was noted in either hepatocytes or fibrous stroma in normal liver and liver cirrhosis tissues (Fig. 1). In focal nodular hyperplasia tissue, a benign liver disease, expression of periostin was not seen in either hepatocytes or fibrous scars (Fig. 1).

In HCC tissue, while no expression of periostin was seen in cancer cells themselves, weak periostin expression was localized in capsule contacting to cancer cells (Fig. 2). Similarly,

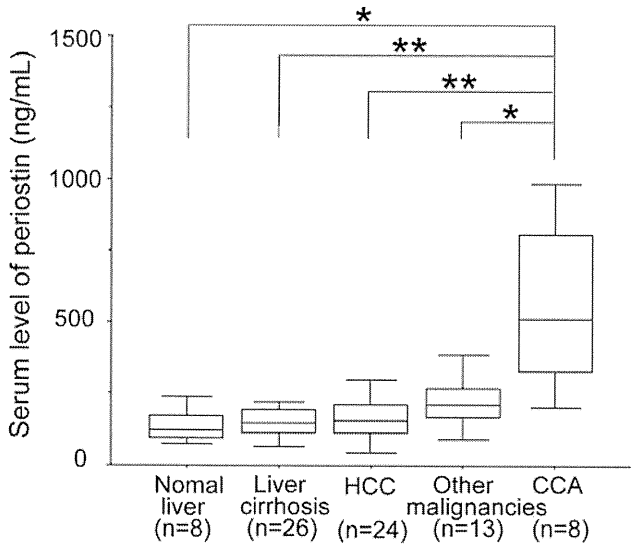

Figure 3. Box plots show serum level of periostin in patients with normal liver and various hepatic malignancies. Serum levels of periostin were measured by newly established a human periostin ELISA assay. The vertical bars indicate the range and the horizontal boundaries of the boxes represent the first and third quartiles. Statistical comparisons among multiple groups were performed by Mann-Whitney U test with Bonferroni correction. *P<0.05 and **P<0.01.

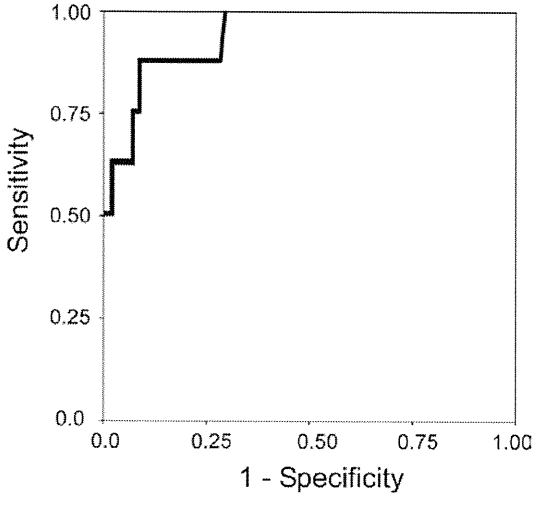

Figure 4. Graph shows receiver operating characteristic (ROC) curves for serum periostin level to distinguish CCA group from other groups. The area under the ROC curve was 0.94. The optimal cut-off value between patients with or without CCA is 302 ng/ml based on the Youden-index.

expression of periostin was detected in a portion of stroma, but not in cancer cells of sarcoma and angiomyolipoma tissues (Fig. 2). Moderate periostin expression was seen in stroma of scirrhous type of HCC, and strong periostin expression was noted in fibrous stroma of CCA tissues (Fig. 2).

Serum periostin levels. With serum periostin levels Kruskal Wallis test showed statistically significant difference (Table I, P<0.001), and multiple pairwaise comparisons revealed that serum periostin level in the CCA group was significantly higher than that in normal liver, liver cirrhosis, HCC, or other malignancies groups (Fig. 3).

Following these results we analyzed the bivariate logistic regression analysis of serum periostin levels to diagnose CCA. A significant association was seen between serum periostin level and CCA group [odds ratio, 1.014; 95% confidence interval (CI), 1.006-1.023; P=0.001].

ROC analyses and diagnostic performances for distinguishing CCA from others. We conducted receiver operating characteristic (ROC) analysis to determine the cut-off value of periostin for distinguishing CCA group from other groups. The area under the ROC curve (AUC) showed statistically significant value [0.94 (95% CI, 0.85-1.00), P=0.001] (Fig. 4). The optimal cut-off value of serum periostin levels was 302 ng/ml based on the Youden index, and respective diagnostic performances for distinguishing CCA from others were shown in Table II: sensitivity, 0.88 (95% CI, 0.47-0.99); specificity, 0.92 (95% CI, 0.83-0.96); accuracy, 0.91 (95% CI, 0.83-0.96); PPV, 0.54 (95% CI, 0.25-0.81); NPV, 0.98 (95% CI, 0.92-0.99); positive-LR, 10.4 (95% CI, 4.8-13.4); and negative-LR, 0.13 (95% CI, 0.03-0.49).

In all of hepatic malignant neoplasms (n=45), the AUC of serum periostin levels for distinguishing CCA from other hepatic malignancies was greater than that of other tumor markers, including AFP, CEA, or CA19-9 (Table III).

Discussion

In this study we demonstrated that pathologically-determined periostin expression was stronger in the fibrous stroma of CCA compared with other hepatic malignancies. In addition, serum periostin level was significantly elevated in patients with CCA and enabled distinction between CCA and other hepatic malignancies.

Periostin occurs in fibrous stroma and plays significant roles in the development, promotion, and progression of various cancers (29). Recently, Riener *et al* and Utispan *et al* reported that periostin expression is seen in the stromal fibroblasts of CCA tissue (16,17). In good accordance with previous reports, high expression of periostin was also noted in the stroma of CCA tissue in this study.

Although the reason and the impact of this up-regulation of periostin in the fibrous stroma of CCA remain unclear, transforming growth factor β (TGF-β) seems to be a key molecule because the expression of periostin is regulated by TGF-β (30). TGF-β is reported to be involved in the cholangiocarcinogenesis (31), growth (32), invasion (33), and epithelial-mesenchymal transition of CCA (34). Thus, increased expression of periostin may be caused by TGF-β and have an impact of the malignant potential of CCA.

In the present study, we also revealed that no periostin expression was seen in normal liver, liver cirrhosis, or focal nodular hyperplasia. Furthermore, we observed that low to moderate expression of periostin was seen in the capsule of HCC tissue and in fibrous stroma of HCC with sarcomatous change. Thus, high expression of periostin was unique to the stroma of CCA. Since periostin is a secretory protein (11,22), these findings let us hypothesize that serum periostin level may enable distinction between CCA and other hepatic malignancies.

Table II. Diagnostic performance of serum periostin levels for distinguishing cholangiocarcinoma from others.

Cut-off value	TP	TN	FN	FP	Sensitivity (95% CI)	Specificity (95% CI)	Accuracy (95% CI)	PPV (95% CI)	NPV (95% CI)	LR^+ (95% CI)	LR^- (95% CI)
302 ng/ml	7	65	1	6	0.88 (0.47-0.99)	0.92 (0.83-0.96)	0.91 (0.83-0.96)	0.54 (0.25-0.81)	0.98 (0.92-0.99)	10.4 (4.8-13.4)	0.13 (0.03-0.49)

TP, true positive; TN, true negative; FN, false negative; FP, false positive; CI, confidence interval; PPV, positive predictive value; NPV, negative predictive value; LR^+, positive likelihood ratio; LR^-, negative likelihood ratio.

Table III. Areas under receiver operating characteristic curves for distinguishing cholangiocarcinoma from other hepatic malignancies.

Serum level of each tumor marker	AUC	95% CI	P-value
AFP	0.760	0.620-0.903	0.021
CEA	0.746	0.568-0.923	0.029
CA19-9	0.631	0.361-0.901	0.244
Periostin	0.936	0.849-1.000	<0.001

AUC, area under receiver operating characteristic curve; CI, confidene interval; AFP, α fetoprotein; CEA, carcinoembryonic antigen; CA19-9, carbohydrate antigen 19-9. Each AUC was measured when finding was positive as follows: differentiating cholangiocarcinoma from other hepatic malignancies was positive when each serum level of CEA, CA19-9, or Periostin was higher than any cut-off values and when serum level of AFP was lower than those.

Serum levels of periostin are evaluated in patients with non-small cell lung carcinoma and breast cancer (12,13). Although serum levels of periostin are associated with disease progression, no studies have compared levels between healthy subjects and cancer patients (12,13). Sasaki *et al* measured serum periostin level in patients with thymoma and reported that there are large overlapping ranges between serum levels of periostin in thymoma patients and controls (35). Therefore, we developed a monoclonal antibody against periostin and established new ELISA for measurement of serum periostin level. Using the new ELISA using monoclonal antibody, we first demonstrated that serum periostin level in patient with CCA was significantly elevated compared to those in patients with normal liver, liver cirrhosis, HCC, and other hepatic malignancies.

We also examine the potential use of serum periostin level as a serodiagnostic marker for CCA. In bivariate logistic regression analysis, serum periostin level was only associated with CCA group. These findings suggest that serum periostin can distinguish CCA group from other groups. In ROC analysis, AUC of serum periostin level showed more than 0.9, indicating a potential of high diagnostic accuracy (28). Moreover, ROC analyses among hepatic malignancies revealed that periostin showed the widest AUC compared to other tumor markers, such as AFP, CEA, and CA19-9. Finally, we examined diagnostic performances of serum periostin level for CCA and found the optimal cut-off value of 302 ng/ml showed acceptable sensitivity, specificity, accuracy, PPV, and NPV. In addition, positive-LR and negative-LR showed more than 10 and between 0.1-0.2, respectively, indicating a potential of clinical practical use (36). Although CA19-9, CEA, and CA-125 are currently the most widely used serum tumor markers for CCA, the sensitivity and specificity of these tumor markers are low (18,37), which consisted with our results. While serum levels of interleukin-6, trypsinogen-2, mucin 5AC, and soluble fragment of cytokeratin 19 are also reported as potential tumor makers, their clinical roles have not yet been elucidated (18,37). These previous reports and our own findings suggest that serum periostin is a novel serodiagnostic marker for CCA.

There were some potential limitations to our study. The study was retrospective and involved a relatively small number of patients. Similarly the cut-off value of serum periostin level was based on small number of patients. A prospective study with a substantially large sample from multiple centers is needed to further validate our findings.

In conclusion, we showed that periostin expression was higher in the fibrous stroma of CCA compared to other hepatic malignancies. Furthermore, serum periostin level was significantly elevated in patients with CCA, thereby, enabling distinction between CCA and other hepatic malignancies.

Acknowledgements

This study was supported, in part, by a Grant-in-Aid for Young Scientists (B) (No. 22790874 to T.K.) and a Grant-in-Aid for Scientific Research (C) (No. 21590865 to M.S.) from the Ministry of Education, Culture, Sports, Science and Technology of Japan, by Health and Labour Sciences Research Grants for Research on Hepatitis from the Ministry of Health, Labour and Welfare of Japan, and by a Grant for Cancer Research from Fukuoka Cancer Society.

References

1. Hamilton DW: Functional role of periostin in development and wound repair: implications for connective tissue disease. J Cell Commun Signal 2: 9-17, 2008.
2. Norris RA, Moreno-Rodriguez R, Hoffman S and Markwald RR: The many facets of the matricelluar protein periostin during cardiac development, remodeling, and pathophysiology. J Cell Commun Signal 3: 275-286, 2009.
3. Snider P, Hinton RB, Moreno-Rodriguez RA, Wang J, Rogers R, Lindsley A, Li F, Ingram DA, Menick D, Field L, Firulli AB, Molkentin JD, Markwald R and Conway SJ: Periostin is required for maturation and extracellular matrix stabilization of noncardiomyocyte lineages of the heart. Circ Res 102: 752-760, 2008.

4. Kii I, Nishiyama T, Li M, Matsumoto K, Saito M, Amizuka N and Kudo A: Incorporation of tenascin-C into the extracellular matrix by periostin underlies an extracellular meshwork architecture. J Biol Chem 285: 2028-2039, 2010.
5. Norris RA, Damon B, Mironov V, Kasyanov V, Ramamurthi A, Moreno-Rodriguez R, Trusk T, Potts JD, Goodwin RL, Davis J, Hoffman S, Wen X, Sugi Y, Kern CB, Mjaatvedt CH, Turner DK, Oka T, Conway SJ, Molkentin JD, Forgacs G and Markwald RR: Periostin regulates collagen fibrillogenesis and the biomechanical properties of connective tissues. J Cell Biochem 101: 695-711, 2007.
6. Takayama G, Arima K, Kanaji T, Toda S, Tanaka H, Shoji S, McKenzie AN, Nagai H, Hotokebuchi T and Izuhara K: Periostin: a novel component of subepithelial fibrosis of bronchial asthma downstream of IL-4 and IL-13 signals. J Allergy Clin Immunol 118: 98-104, 2006.
7. Maruhashi T, Kii I, Saito M and Kudo A: Interaction between periostin and BMP-1 promotes proteolytic activation of lysyl oxidase. J Biol Chem 285: 13294-13303, 2010.
8. Ruan K, Bao S and Ouyang G: The multifaceted role of periostin in tumorigenesis. Cell Mol Life Sci 66: 2219-2230, 2009.
9. Bao S, Ouyang G, Bai X, Huang Z, Ma C, Liu M, Shao R, Anderson RM, Rich JN and Wang XF: Periostin potently promotes metastatic growth of colon cancer by augmenting cell survival via the Akt/PKB pathway. Cancer Cell 5: 329-339, 2004.
10. Baril P, Gangeswaran R, Mahon PC, Caulee K, Kocher HM, Harada T, Zhu M, Kalthoff H, Crnogorac-Jurcevic T and Lemoine NR: Periostin promotes invasiveness and resistance of pancreatic cancer cells to hypoxia-induced cell death: role of the beta4 integrin and the PI3k pathway. Oncogene 26: 2082-2094, 2007.
11. Kanno A, Satoh K, Masamune A, Hirota M, Kimura K, Umino J, Hamada S, Satoh A, Egawa S, Motoi F, Unno M and Shimosegawa T: Periostin, secreted from stromal cells, has biphasic effect on cell migration and correlates with the epithelial to mesenchymal transition of human pancreatic cancer cells. Int J Cancer 122: 2707-2718, 2008.
12. Sasaki H, Dai M, Auclair D, Fukai I, Kiriyama M, Yamakawa Y, Fujii Y and Chen LB: Serum level of the periostin, a homologue of an insect cell adhesion molecule, as a prognostic marker in non-small cell lung carcinomas. Cancer 92: 843-848, 2001.
13. Sasaki H, Yu CY, Dai M, Tam C, Loda M, Auclair D, Chen LB and Elias A: Elevated serum periostin levels in patients with bone metastases from breast but not lung cancer. Breast Cancer Res Treat 77: 245-252, 2003.
14. Shao R, Bao S, Bai X, Blanchette C, Anderson RM, Dang T, Gishizky ML, Marks JR and Wang XF: Acquired expression of periostin by human breast cancers promotes tumor angiogenesis through up-regulation of vascular endothelial growth factor receptor 2 expression. Mol Cell Biol 24: 3992-4003, 2004.
15. Okamura N, Yoshida M, Shibuya A, Sugiura H, Okayasu I and Ohbu M: Cellular and stromal characteristics in the scirrhous hepatocellular carcinoma: comparison with hepatocellular carcinomas and intrahepatic cholangiocarcinomas. Pathol Int 55: 724-731, 2005.
16. Riener MO, Fritzsche FR, Soll C, Pestalozzi BC, Probst-Hensch N, Clavien PA, Jochum W, Soltermann A, Moch H and Kristiansen G: Expression of the extracellular matrix protein periostin in liver tumours and bile duct carcinomas. Histopathology 56: 600-606, 2010.
17. Utispan K, Thuwajit P, Abiko Y, Charngkaew K, Paupairoj A, Chau-in S and Thuwajit C: Gene expression profiling of cholangiocarcinoma-derived fibroblast reveals alterations related to tumor progression and indicates periostin as a poor prognostic marker. Mol Cancer 9: 13, 2010.
18. Khan SA, Davidson BR, Goldin R, Pereira SP, Rosenberg WM, Taylor-Robinson SD, Thillainayagam AV, Thomas HC, Thursz MR, Wasan H and British Society of Gastroenterology: Guidelines for the diagnosis and treatment of cholangiocarcinoma: consensus document. Gut 51 (Suppl. 6): VI1-9, 2002.
19. Khan SA, Thomas HC, Davidson BR and Taylor-Robinson SD: Cholangiocarcinoma. Lancet 366: 1303-1314, 2005.
20. Meza-Junco J, Montano-Loza AJ, Ma M, Wong W, Sawyer MB and Bain VG: Cholangiocarcinoma: has there been any progress? Can J Gastroenterol 24: 52-57, 2010.
21. Nakeeb A and Pitt HA: Radiation therapy, chemotherapy and chemoradiation in hilar cholangiocarcinoma. HPB (Oxford) 7: 278-282, 2005.
22. Oku E, Kanaji T, Takata Y, Oshima K, Seki R, Morishige S, Imamura R, Ohtsubo K, Hashiguchi M, Osaki K, Yakushiji K, Yoshimoto K, Ogata H, Hamada H, Izuhara K, Sata M and Okamura T: Periostin and bone marrow fibrosis. Int J Hematol 88: 57-63, 2008.
23. World Medical Association Declaration of Helsinki: Ethical Principles for Medical Research Involving Human Subjects 2008 version (59th World Medical Association General Assembly, Seoul, October 2008); http://www.wma.net/en/30publications/10policies/b3/index.html
24. Hayashi N, Yoshimoto T, Izuhara K, Matsui K, Tanaka T and Nakanishi K: T helper 1 cells stimulated with ovalbumin and IL-18 induce airway hyperresponsiveness and lung fibrosis by IFN-gamma and IL-13 production. Proc Natl Acad Sci USA 104: 14765-14770, 2007.
25. Kawaguchi T, Sakisaka S, Sata M, Mori M and Tanikawa K: Different lobular distributions of altered hepatocyte tight junctions in rat models of intrahepatic and extrahepatic cholestasis. Hepatology 29: 205-216, 1999.
26. Kawaguchi T, Sakisaka S, Mitsuyama K, Harada M, Koga H, Taniguchi E, Sasatomi K, Kimura R, Ueno T, Sawada N, Mori M and Sata M: Cholestasis with altered structure and function of hepatocyte tight junction and decreased expression of canalicular multispecific organic anion transporter in a rat model of colitis. Hepatology 31: 1285-1295, 2000.
27. Kawaguchi T, Ide T, Taniguchi E, Hirano E, Itou M, Sumie S, Nagao Y, Yanagimoto C, Hanada S, Koga H and Sata M: Clearance of HCV improves insulin resistance, beta-cell function, and hepatic expression of insulin receptor substrate 1 and 2. Am J Gastroenterol 102: 570-576, 2007.
28. Swets JA: Measuring the accuracy of diagnostic systems. Science 240: 1285-1293, 1988.
29. Kudo Y, Siriwardena BS, Hatano H, Ogawa I and Takata T: Periostin: novel diagnostic and therapeutic target for cancer. Histol Histopathol 22: 1167-1174, 2007.
30. Horiuchi K, Amizuka N, Takeshita S, Takamatsu H, Katsuura M, Ozawa H, Toyama Y, Bonewald LF and Kudo A: Identification and characterization of a novel protein, periostin, with restricted expression to periosteum and periodontal ligament and increased expression by transforming growth factor beta. J Bone Miner Res 14: 1239-1249, 1999.
31. Yokomuro S, Tsuji H, Lunz JG III, Sakamoto T, Ezure T, Murase N and Demetris AJ: Growth control of human biliary epithelial cells by interleukin 6, hepatocyte growth factor, transforming growth factor beta1, and activin A: comparison of a cholangiocarcinoma cell line with primary cultures of non-neoplastic biliary epithelial cells. Hepatology 32: 26-35, 2000.
32. Miyazaki M, Ohashi R, Tsuji T, Mihara K, Gohda E and Namba M: Transforming growth factor-beta 1 stimulates or inhibits cell growth via down- or up-regulation of p21/Waf1. Biochem Biophys Res Commun 246: 873-880, 1998.
33. Shen FZ, Zhang BY, Feng YJ, Jia ZX, An B, Liu CC, Deng XY, Kulkarni AD and Lu Y: Current research in perineural invasion of cholangiocarcinoma. J Exp Clin Cancer Res 29: 24, 2010.
34. Sato Y, Harada K, Itatsu K, Ikeda H, Kakuda Y, Shimomura S, Shan Ren X, Yoneda N, Sasaki M and Nakanuma Y: Epithelial-mesenchymal transition induced by transforming growth factor-{beta}1/snail activation aggravates invasive growth of cholangiocarcinoma. Am J Pathol 177: 141-152, 2010.
35. Sasaki H, Dai M, Auclair D, Kaji M, Fukai I, Kiriyama M, Yamakawa Y, Fujii Y and Chen LB: Serum level of the periostin, a homologue of an insect cell adhesion molecule, in thymoma patients. Cancer Lett 172: 37-42, 2001.
36. Jaeschke R, Guyatt GH and Sackett DL: Users' guides to the medical literature. III. How to use an article about a diagnostic test. B. What are the results and will they help me in caring for my patients? The Evidence-Based Medicine Working Group. JAMA 271: 703-707, 1994.
37. Gatto M, Bragazzi MC, Semeraro R, Napoli C, Gentile R, Torrice A, Gaudio E and Alvaro D: Cholangiocarcinoma: update and future perspectives. Dig Liver Dis 42: 253-260, 2010.

Evaluation of the Mean and Entropy of Apparent Diffusion Coefficient Values in Chronic Hepatitis C: Correlation with Pathologic Fibrosis Stage and Inflammatory Activity Grade[1]

Kiminori Fujimoto, MD, PhD
Tatsuyuki Tonan, MD
Sanae Azuma, MD
Masayoshi Kage, MD, PhD
Osamu Nakashima, MD, PhD
Takeshi Johkoh, MD, PhD
Naofumi Hayabuchi, MD, PhD
Koji Okuda, MD, PhD
Takumi Kawaguchi, MD, PhD
Michio Sata, MD, PhD
Aliya Qayyum, MBBS

Purpose: To determine whether mean and entropy apparent diffusion coefficient (ADC) values obtained at diffusion-weighted (DW) magnetic resonance (MR) imaging can help detect and stage histopathologic liver fibrosis and grade inflammation activity in patients with chronic hepatitis C.

Materials and Methods: This retrospective study was approved by the institutional review board, and the requirement for informed consent was waived. The study included 55 patients with focal hepatic lesions and either chronic hepatitis C (n = 43) or normal hepatic function (control subjects) (n = 12). Mean and entropy of volume histograms were generated in four cubic regions of interest placed in the right hepatic lobe of ADC map images, which were obtained at echo-planar DW MR imaging (gradient factor b values of 0 and 1000 sec/mm^2). These two parameters (mean and entropy ADC) were compared by using METAVIR histopathologic liver fibrosis and inflammatory activity scores. Statistical analysis was performed with the Kruskal-Wallis test and receiver operating characteristic curves.

Results: The mean ADC decreased with an increase in the fibrosis stage or inflammatory activity grade, and the entropy ADC increased with an increase in the fibrosis stage or inflammatory activity grade ($P < .001$ for all comparisons, Kruskal-Wallis test). The area under the receiver operating characteristic curve (A_z) for the mean ADC was statistically significant in the differentiation of fibrosis stage or inflammatory activity grade (A_z, 0.807–0.926; $P < .001$ for all comparisons). Entropy of ADC was helpful for classifying normal from abnormal fibrosis stage or inflammatory activity grade (A_z for both parameters, 0.937; $P < .001$).

Conclusion: Assessment of a combination of mean ADC and entropy ADC in patients with chronic hepatitis C is more accurate for predicting pathologic hepatic fibrosis stage and inflammatory activity grade and helpful for detecting early fibrotic or inflammatory activity when compared with assessment of mean ADC alone.

[1] From the Departments of Radiology (K.F., T.T., S.A., N.H.), Diagnostic Pathology (M.K.), Pathology (O.N.), Surgery (K.O.), and Digestive Disease Information and Research (T.K., M.S.), Kurume University School of Medicine, 67 Asahi-machi, Kurume, 830-0011 Japan; Center for Diagnostic Imaging, Kurume University Hospital, Kurume, Japan (K.F.); Department of Radiology, Kinki Central Hospital of Mutual Aid Association of Public School Teachers, Itami, Japan (T.J.); and Department of Radiology, University of California–San Francisco, San Francisco, Calif (A.Q.).
Received April 27, 2010; revision requested June 18; revision received August 16; accepted September 8; final version accepted October 1. **Address correspondence to** K.F. (e-mail: *kimichan@med.kurume-u.ac.jp*).

It is estimated that approximately 400 million people worldwide are infected with the hepatitis C virus (1), with chronic infection in 75%–85% of patients. Once a diagnosis of chronic hepatitis C virus infection is established, cirrhosis develops within 10–20 years in approximately 20% of patients (2). Approximately 50% of patients with chronic hepatitis C fail to achieve a sustained virologic response to standard therapy with PEGylated interferon and ribavirin (3). Disease progression, which may lead to hepatic decompensation, hepatocellular carcinoma, and death, is particularly common in these patients (4,5).

The severity of liver inflammation and fibrosis in patients with chronic hepatitis C is important to consider when making therapeutic decisions and is a useful prognostic indicator. Liver biopsy is the current reference standard used in the assessment of hepatic necroinflammation and fibrosis (6). Several histologic scoring systems are used to evaluate chronic viral hepatitis (7–10). Of these, the METAVIR scoring system was specially designed for determining hepatic fibrosis stage in patients with chronic hepatitis C (10,11). The current focus in clinical practice, however, has shifted from diagnosis alone to risk stratification and disease monitoring (12,13). Liver biopsy is invasive, with a recognized morbidity and mortality, and as such repeated biopsy for the purpose of monitoring disease progression is not the best option. Furthermore, liver biopsies have several inherent limitations, such as sampling error and interobserver variability (6).

Several noninvasive techniques, including biochemical and hematologic tests, a scoring system using a combination of clinical and laboratory tests, ultrasonography (US)–based transient elastography (6,14), and magnetic resonance (MR) imaging (15–24), have been evaluated. Among these, diffusion-weighted (DW) MR imaging has shown promise in the detection and quantification of hepatic fibrosis (18–24) but has not yet been validated as a marker for pathologic hepatic necroinflammation. To our knowledge, semiquantitative analysis of DW MR imaging in the assessment of liver fibrosis has mainly been evaluated by determining the mean apparent diffusion coefficient (ADC) values of regions of interest in liver parenchyma, but volume histogram analyses have not been evaluated. Entropy describes the variation in a volume histogram of ADC and has been shown to have clinical utility for evaluating morphologic changes of organ tissues outside the abdomen (25,26). We postulated that the mean hepatic ADC values and the entropy of hepatic ADC (entropy ADC) values would be helpful for evaluating the alteration in hepatic parenchyma in chronic hepatitis C.

The purpose of this study was to determine whether the mean and entropy ADC values obtained with DW MR imaging can help detect and stage histopathologic liver fibrosis and grade inflammatory activity in patients with chronic hepatitis C.

Advance in Knowledge

- In patients with chronic hepatitis C, entropy of apparent diffusion coefficient (ADC) values might be a sensitive marker for the detection of early hepatic inflammatory activity (median entropy ADC value was 1.23 for an inflammatory activity score of A0 [no activity] and ranged from 1.48 to 1.57 for inflammatory activity scores of A1–A3 [mild to severe activity]) and fibrosis stage (median entropy ADC value was 1.24 for grade F0 fibrosis [no fibrosis] and ranged from 1.36 to 1.64 for grades F1–F4 fibrosis [minimal fibrosis to cirrhosis]).

Implication for Patient Care

- Evaluation of the mean and entropy of liver ADC values obtained with diffusion-weighted MR imaging is a noninvasive method for assessing liver fibrosis stage and inflammatory activity grade and might be used to differentiate early from advanced chronic liver disease; its noninvasiveness allows for repeat performance.

Materials and Methods

Patients

The institutional review board approved this retrospective study and waived the requirement to obtain patient approval or informed consent for the retrospective review of their records and images, which complied with the principles of the Declaration of Helsinki (2008 version) of the World Medical Association (27).

We retrospectively reviewed the medical records and MR images from all patients who underwent assessment of suspected focal hepatic lesions at our institution between June 2006 and May 2007 and who fulfilled the following inclusion criteria: *(a)* patients underwent DW MR imaging, *(b)* pathologic specimens obtained at liver biopsy were adequate for determining the METAVIR score, and *(c)* patients had either chronic active hepatitis C or absence of hepatic dysfunction or viral hepatitis. The patients with an absence of hepatic dysfunction or viral hepatitis were used as control subjects. Chronic active hepatitis C was defined as an established diagnosis of chronic hepatitis C virus infection with detectable anti–hepatitis C virus antibodies and detectable serum

Published online before print
10.1148/radiol.10100853

Radiology 2011; 258:739–748

Abbreviations:
ADC = apparent diffusion coefficient
A_z = area under the receiver operating characteristic curve
CI = confidence interval
DW = diffusion weighted
IQR = 25th to 75th percentile of the interquartile range

Author contributions:
Guarantors of integrity of entire study, K.F., T.T., M.K.; study concepts/study design or data acquisition or data analysis/interpretation, all authors; manuscript drafting or manuscript revision for important intellectual content, all authors; manuscript final version approval, all authors; literature research, K.F., T.T., M.K., T.J., T.K.; clinical studies, K.F., T.T., S.A., M.K., O.N., T.J., N.H., K.O., T.K., M.S.; statistical analysis, K.F.; and manuscript editing, K.F., A.Q.

Potential conflicts of interest are listed at the end of this article.

hepatitis C virus RNA in conjunction with serum aminotransferase levels that remained abnormally high for more than 6 months. Patients were excluded if they had *(a)* a life-threatening extrahepatic condition and *(b)* other causes of chronic liver disease (eg, hepatitis B virus, excessive alcohol consumption [>30 g per day], hemochromatosis, autoimmune hepatitis, Wilson disease, α_1-antitrypsin deficiency, primary sclerosing cholangitis, or primary biliary cirrhosis).

We identified 84 patients who underwent DW MR imaging and METAVIR scoring at our institution. Twenty-nine of those 84 patients were excluded because their chronic liver disease was due to a cause other than the hepatitis C virus (hepatitis B virus in 17 patients and excessive alcohol consumption in 12). Therefore, our final patient population consisted of 55 subjects, including 43 patients with chronic hepatitis C and 12 control subjects without hepatic dysfunction or viral hepatitis. Patients ranged in age from 34 to 83 years (median age, 65 years) and included 35 men and 20 women. The median patient age was 63 years (25th to 75th percentile of the interquartile range [IQR], 59–73 years) for men and 69 years (IQR, 55–72 years) for women. There was no statistically significant difference in age distribution according to sex ($P = .255$, Mann-Whitney U test).

In 48 of the 55 patients (36 patients with chronic hepatitis C and the 12 control subjects), pathologic assessment of the liver was performed by means of surgical biopsy at resection of the focal hepatic lesions (eg, hepatocellular carcinoma or hepatic metastases). In seven of the 55 patients, pathologic assessment of the liver was performed by means of US-guided biopsy with a 17-gauge core biopsy needle. The median interval between DW MR imaging and surgical or core liver biopsy was 7 days (range, 1–14 days).

MR Imaging Techniques and Interpretation

MR imaging was performed at a field strength of 1.5 T (Magnetom Symphony Advanced; Siemens, Erlangen, Germany) with use of a body phased-array coil.

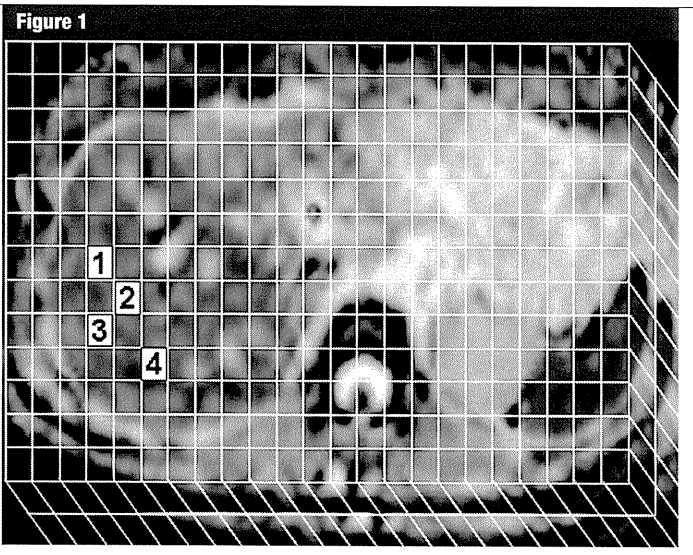

Figure 1: Image illustrates the method used to measure regions of interest on an ADC map. With use of computer software (developed in-house by authors), two independent observers freely and easily selected a region of interest by clicking a mesh unit on the right hepatic lobe of an ADC map image while avoiding the large vessels, focal hepatic lesions, or artifacts. Four cubic regions of interest (3.6 cm^3, approximately 36 voxels) were chosen for liver parenchyma. Numbers on image are regions of interest.

After routine T1- and T2-weighted imaging was performed for the assessment of focal hepatic lesions, a series of respiratory-triggered DW MR images was obtained in all patients.

DW MR imaging was performed in the transverse plane by combining single-shot spin-echo echo-planar imaging with a chemical shift–selective pulse. The imaging parameters for DW MR imaging were as follows: repetition time, 2000 msec; echo time, 81 msec; directions of the motion-probing gradient, three orthogonal axes; gradient factor b values of 0 and 1000 sec/mm^2; 2170-Hz per pixel bandwidth; 350-mm field of view; 128 × 88 rectangular matrixes; 9-mm-thick sections; 1-mm intersection gap; four signals acquired; and acquisition time of approximately 1 minute 30 seconds.

Liver ADC was calculated by using the following equation: $ADC = (-1/b) \times \ln (S_b/S_0)$, where b is the diffusion-sensitizing factor (b value), and S_b and S_0 the signal intensity with and without diffusion weighting, respectively. ADC maps were constructed according to this equation on the basis of a voxelwise calculation.

All regions of interest were determined by two independent observers (T.T. and S.A., with 12 and 8 years of experience, respectively) by using plug-in software developed in-house by two of the authors (K.F. and T.J.) (Fig 1). The two observers were abdominal radiologists who knew that all patients in the study had focal hepatic lesions but were blinded to the other clinical information. Four separate cubic regions of interest (3.6 cm^3, approximately 36 voxels) were manually placed in the anterior and posterior segments of the right hepatic lobe at the level of the porta hepatis (whenever possible) on the calculation ADC maps; care was taken to avoid focal lesions, major vascular structures, and artifacts such as chemical shifts, magnetic susceptibility, and cardiac motion. The regions of interest were drawn in the right hepatic lobe to approximate the regions expected to be sampled for histologic examination.

The entropy ADC values of the selected regions of interest, which were calculated by using the volume histogram method (24,25), were obtained automatically from the same plug-in software. Entropy describes the variation in an ADC histogram such that a large variation in hepatic ADC is associated with larger entropy values.

The histogram entropy was calculated as follows:

$$\text{Entropy} = \sum (-p_i) \log(p_i),$$

where p_i represents the probability of ADC value in the image and is calculated by dividing the number of voxels in each ADC value by the number of voxels in all ADC values.

Therefore, ADC values were recorded as the mean and entropy ADC of the volume histogram obtained from the selected regions of interest.

Assessment of Pathologic Specimens

Resected liver specimens (n = 48) and liver biopsy specimens (n = 7) were fixed in formalin, embedded in paraffin, and stained with hematoxylin and eosin. All specimens (n = 55) were retrospectively reviewed independently by two pathologists (M.K. and O.N., with 34 and 26 years of experience, respectively, and subspecialty expertise in liver pathology). The pathologists were blinded to clinical and imaging data.

The fibrosis stage and the necroinflammatory activity grade were evaluated semiquantitatively by using the METAVIR scoring system (9,13,20). Fibrosis was graded on a scale of 0 to 4, as follows: F0 = no fibrosis, F1 = portal fibrosis without septa, F2 = portal fibrosis and few septa, F3 = numerous septa without cirrhosis, and F4 = cirrhosis. The necroinflammatory activity score was graded on a scale of 0 to 3, as follows: A0 = no activity, A1 = mild activity, A2 = moderate activity, and A3 = severe activity. After calculating the κ values for interobserver agreement on the basis of the independent readings, any cases in which the final fibrosis stage or activity grade differed between the two pathologists were reevaluated and scored in consensus.

Statistical Analysis

The mean and entropy ADC values of the two independent observers' measurements were compared with the Bland-Altman method (28,29). The coefficients of repeatability were calculated as 1.96 times the standard deviation of the differences between the two measurements made by the two observers. The linear correlation coefficient (r value) of each difference of measurement was calculated by using Pearson linear regression analysis, and the estimated bias (ie, the mean difference between two observers' measurements) was assessed.

Agreement between the two pathologists with regard to the fibrosis stage and inflammatory activity grade was assessed by using κ statistics (30) with use of the diagnoses made before agreement by consensus. The strength of the interobserver agreement indicated with κ values was classified as follows: poor, $\kappa < 0.0$; slight, κ = 0.0–0.20; fair, κ = 0.21–0.40; moderate, κ = 0.41–0.60; substantial, κ = 0.61–0.80; and almost perfect, κ = 0.81–1.00 (31). The relationship between the fibrosis stage and inflammatory activity grade in patients with chronic hepatitis C was assessed by using the Spearman correlation test.

The Kruskal-Wallis test was used to determine the statistical significance of intergroup differences in the pathologic scores with mean and entropy ADC. In case of statistical significance, multiple pairwise comparisons were conducted with the Mann-Whitney U test with Bonferroni correction.

The diagnostic performance of mean or entropy ADC in predicting the fibrotic stage or inflammatory activity grade was assessed with use of the area under the receiver operating characteristic curve (A_z) (32). Sensitivity, specificity, positive and negative predictive values, and positive and negative likelihood ratios (33,34) for the classification of F0 versus F1–F4 fibrosis (score ≥F1); F0 and F1 versus F2–F4 fibrosis (score ≥F2); F0–F2 versus F3 and F4 fibrosis (score ≥F3); or F0–F3 versus F4 fibrosis (score = F4) and for the classification of A0 versus A1–A3 activity (grade ≥A1); A0 and A1 versus A2 and A3 activity (grade ≥A2); or A0–A2 versus A3 activity (grade = A3) were calculated with standard formulas according to the values of these indexes and with varied index values that indicated positive differentiation (ie, threshold values).

All analyses were performed with statistical software (SPSS, version 12.0J; SPSS, Chicago, Ill), and $P < .05$ was considered indicative of a statistically significant difference.

Results

Interobserver Agreement

There was no significant difference between measurements made by the two observers for the two parameters; the interclass Pearson correlation coefficients were 0.98 (95% confidence interval [CI]: 0.95, 1.0) for mean ADC and 0.97 (95% CI: 0.94, 1.0) for entropy ADC; the mean difference (±standard deviation) was −0.004 ± 0.05 for mean ADC and −0.013 ± 0.037 for entropy ADC; and the coefficients of repeatability were 0.100 for mean ADC and 0.072 for entropy ADC. Bland-Altman plots with 95% limits of agreement for mean and entropy ADC are shown in Figure 2a and Figure 2b, respectively. There was no proportional bias or fixed bias in each Bland-Altman plot for the two parameters.

There was substantial agreement between the two independent pathologists with regard to fibrosis stage (κ = 0.73; 95% CI: 0.59, 0.86) and inflammatory activity grade (κ = 0.74; 95% CI: 0.60, 0.88). None of the 12 control subjects had any signs of fibrosis or inflammatory activity because they did not have hepatic impairment. At the consensus reading, stage F0 fibrosis was diagnosed in 12 of the 55 patients (22%), stage F1 fibrosis in nine (16%), stage F2 fibrosis in 11 (20%), stage F3 fibrosis in 11 (20%), and stage F4 fibrosis in 12 (22%), showing a homogeneous distribution of fibrosis stages. The inflammatory activity grade was A0 in 12 of the 55 patients (22%), A1 in 13 (24%), A2 in 17 (31%), and A3 in 13 (24%). In the 43 patients with chronic hepatitis C, a significant correlation

Figure 2

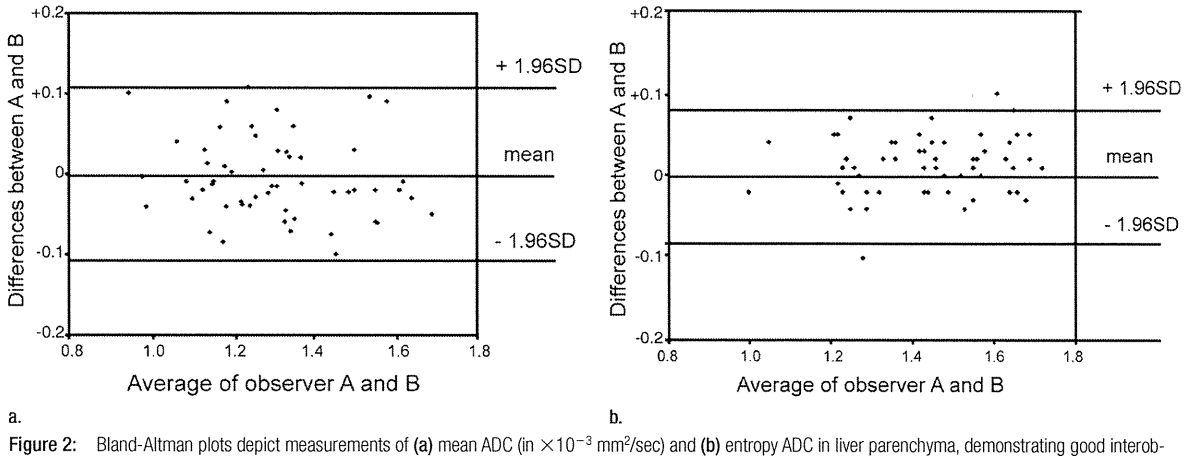

Figure 2: Bland-Altman plots depict measurements of **(a)** mean ADC (in $\times 10^{-3}$ mm²/sec) and **(b)** entropy ADC in liver parenchyma, demonstrating good interobserver agreement and lack of proportional bias or fixed bias. The average of the measurements made by the two observers is plotted against the difference between the measurements made by the two observers. The thin lines represent the mean value of all differences between the two observers, and the thick lines represent the 95% limits of agreement. *SD* = standard deviation.

was observed between the final fibrosis score and the final inflammatory activity grade ($r = 0.46$, $P = .002$, Spearman correlation test).

Relationship between ADC Parameters and Pathologic Fibrosis Stage

The median mean ADC values according to fibrosis stage were as follows: F0, 1.53×10^{-3} mm²/sec (IQR, $1.35–1.60 \times 10^{-3}$ mm²/sec); F1, 1.45×10^{-3} mm²/sec (IQR, $1.34–1.51 \times 10^{-3}$ mm²/sec); F2, 1.29×10^{-3} mm²/sec (IQR, $1.23–1.34 \times 10^{-3}$ mm²/sec); F3, 1.17×10^{-3} mm²/sec (IQR, $1.14–1.25 \times 10^{-3}$ mm²/sec); and F4, 1.15×10^{-3} mm²/sec (IQR, $1.01–1.26 \times 10^{-3}$ mm²/sec) (Fig 3a). The median entropy ADC values according to fibrosis stage were as follows: F0, 1.24 (IQR, 1.21–1.27); F1, 1.36 (IQR, 1.30–1.49); F2, 1.46 (IQR, 1.35–1.55); F3, 1.55 (IQR, 1.45–1.61); and F4, 1.64 (IQR, 1.45–1.68) (Fig 3b).

The mean ADC decreased with an increase in the stage of liver fibrosis ($P < .001$, Kruskal-Wallis test; Fig 3a). Conversely, the entropy ADC increased with an increase in fibrosis stage ($P < .001$, Kruskal-Wallis test; Fig 3b).

For the mean ADC, there were statistically significant differences in the pairwise comparisons (with Bonferroni correction) of stages of liver fibrosis, as follows: F0 versus F2, $P = .01$; F0 versus F3, $P < .01$; F0 versus F4, $P < .01$; F1 versus F3, $P < .01$; F1 versus F4, $P < .01$; F2 versus F3, $P = .04$; and F2 versus F4, $P = .04$ (Fig 3a). For the entropy ADC, there were statistically significant differences in the pairwise comparisons (Bonferroni correction) of stages of liver fibrosis, as follows: F0 versus F1, $P < .01$; F0 versus F2, $P < .01$; F0 versus F3, $P < .01$; and F1 versus F4, $P = .04$ (Fig 3b).

Relationship between ADC Parameters and Pathologic Inflammatory Activity Grade

The median mean ADC values according to inflammatory activity grade were as follows: A0, 1.53×10^{-3} mm²/sec (IQR, $1.36–1.60 \times 10^{-3}$ mm²/sec); A1, 1.30×10^{-3} mm²/sec (IQR, $1.21–1.51 \times 10^{-3}$ mm²/sec); A2, 1.26×10^{-3} mm²/sec (IQR, $1.19–1.34 \times 10^{-3}$ mm²/sec); and A3, 1.15×10^{-3} mm²/sec (IQR, $1.04–1.22 \times 10^{-3}$ mm²/sec) (Fig 4a). The median entropy ADC values according to activity grade were as follows: A0, 1.23 (IQR, 1.21–1.27); A1, 1.48 (IQR, 1.43–1.64); A2, 1.44 (IQR, 1.33–1.55); and A3, 1.57 (IQR, 1.50–1.67) (Fig 4b).

The mean ADC decreased with an increase in the inflammatory activity grade ($P < .001$, Kruskal-Wallis test; Fig 4a), and the entropy ADC increased with an increase in the inflammatory activity grade ($P < .001$, Kruskal-Wallis test; Fig 4b).

The mean ADC significantly differed between activity grades A0 and A2 and between activity grades A0 and A3 ($P < .01$ for both comparisons, Bonferroni correction) (Fig 4a). The entropy ADC significantly differed between inflammatory activity grade A0 and activity grades A1, A2, and A3 ($P < .01$ for all comparisons, Bonferroni correction) (Fig 4b).

Receiver Operating Characteristic Analyses and Diagnostic Performances for Predicting Pathologic Fibrosis and Activity Scores

The A_z values for mean and entropy ADCs according to different fibrosis and inflammatory activity thresholds are shown in Tables 1 and 2. Optimal cutoff values for mean and entropy ADC, along with the respective diagnostic performances, are shown in Tables 3 and 4.

The A_z for mean ADC was larger than that for entropy ADC in the classification of fibrosis of grade F2 or higher, fibrosis of grade F3 or higher, and fibrosis of grade F4 (Table 1). In

Figure 3

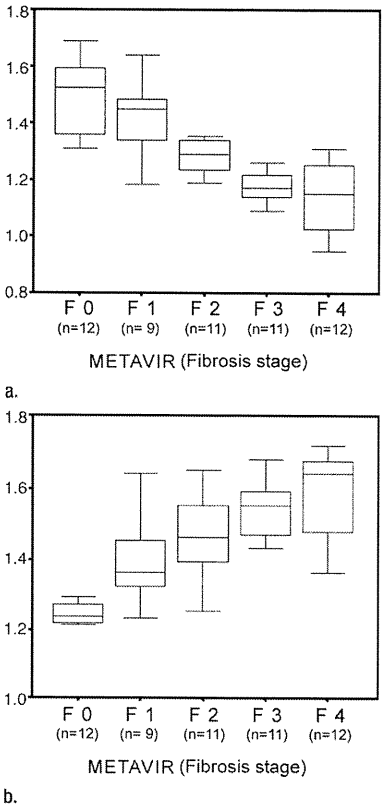

Figure 3: Box plots of **(a)** mean ADC (in $\times 10^{-3}$ mm²/sec) and **(b)** entropy ADC values in liver parenchyma according to METAVIR fibrosis score. The line in each box represents the median, and the horizontal boundaries of the boxes represent the first and third quartiles. The vertical error bars show the minimum and maximum values (range).

Figure 4

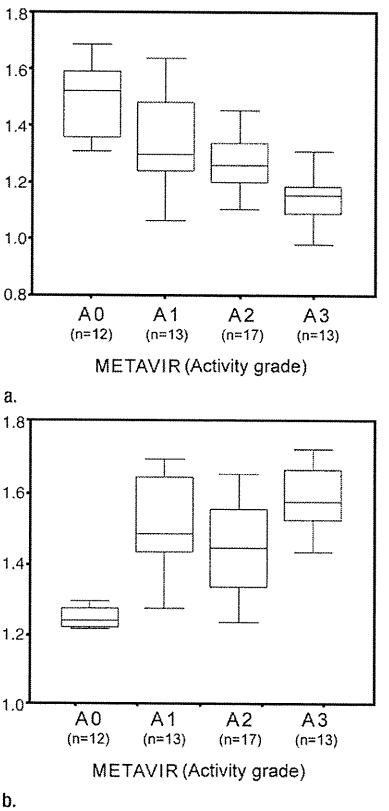

Figure 4: Box plots of **(a)** mean ADC (in $\times 10^{-3}$ mm²/sec) and **(b)** entropy ADC values in liver parenchyma according to METAVIR inflammatory activity score. The line in each box represents the median, and the horizontal boundaries of the boxes represent the first and third quartiles. The vertical error bars show the minimum and maximum values (range).

particular, diagnostic performances in the classification of grade F2 or higher fibrosis and grade F3 or higher fibrosis were quite good (cutoff values of 1.32 and 1.27 $\times$ 10^{-3} mm²/sec resulted in positive likelihood ratios of 9.0 and 5.6, respectively, and negative likelihood ratios of 0.16 and 0.15) (Table 3). Conversely, in the classification of fibrosis of grade F1 or higher, the A_z of entropy ADC was larger than that of mean ADC (Table 1). Thus, with regard to the diagnostic performance, entropy ADC was the most accurate parameter in the classification of grade F1 or higher fibrosis (cutoff value of 1.30 resulted in a positive likelihood ratio of 10.6 and negative likelihood ratio of 0.13). Similarly, the A_z of mean ADC was larger than that of entropy ADC in the classification of inflammatory activity of grade A2 or higher and grade A3 or higher. For inflammatory activity of at least grade A1, the A_z of entropy ADC was larger than that of mean ADC (Table 2). With regard to the diagnostic performance, entropy ADC was the most accurate parameter in the classification of inflammatory activity of grade A1 or higher (cutoff value of 1.30 resulted in a positive likelihood ratio of 10.9 and negative likelihood ratio of 0.10), and mean ADC was a relatively significant predictor for classification of grade A3 inflammatory activity (cutoff value of 1.19 $\times$ 10^{-3} mm²/sec resulted in a positive likelihood ratio of 4.6 and negative likelihood ratio of 0.28) (Table 4).

Discussion

Early studies assessing the relationship between hepatic fibrosis stage and ADC values in the liver reported that a significant correlation was not achieved when using low *b* values (eg, 0–128 sec/mm² and 50–400 sec/mm²) (15,18,19) because DW MR imaging with a low *b* value was influenced by perfusion contamination. Taouli et al (20) reported that the ADC value acquired from *b* values of at least 500 sec/mm² showed a significant correlation with the liver fibrosis stage and that the ADC value with a combination of *b* values of 0–1000 sec/mm² showed the highest significant correlation with fibrosis stage. On the basis of the study of combined ADC measurement with multiple *b* values (0, 200, 400, 800 sec/mm²), Luciani et al (35) reported that ADC changes observed in liver cirrhosis (METAVIR fibrosis score, F4) were more reflective of an alteration in microperfusion than of true diffusion. Although the use of multiple *b* values (intravoxel incoherent motion) may be helpful for differentiating the relative effect of altered microperfusion from that of true diffusion due to increased barriers to water movement, as suggested by Luciani et al, our results are consistent with those of other studies (15,20,21) that demonstrated that liver ADC derived from a combination of *b* values of 0 and 1000 sec/mm² is helpful for predicting hepatic fibrosis. The different correlations of ADC parameters and pathologic findings in our study compared with that of Luciani et al (35) may be explained in part by different patient populations; the patient population in the study by Luciani et al consisted of patients with cirrhosis (12 patients

with grade F4 fibrosis). Further studies (including those performed in patients with chronic hepatitis with a fibrosis score lower than F4) are needed to confirm these findings and shed light on the exact mechanism of diffusion changes observed in liver fibrosis (22).

Previous studies have reported a range of liver ADC sensitivities of 0.74–0.89 and specificities of 0.73–0.87 in the detection of moderate fibrosis (stage F2 or higher) (15,19,21). These findings concur with our observation of mean ADC sensitivity (0.85) and specificity (0.91); however, we observed a greater specificity (0.92) with entropy ADC when including even early liver fibrosis.

Although Lewin et al (15) and Taouli et al (21) reported weak negative correlations between ADC values and the degree of necroinflammation, with a sensitivity of 0.75 and a specificity of 0.78, we observed a stronger negative correlation between mean ADC and inflammatory activity grade (sensitivity, 0.81; specificity, 0.83). In addition, entropy, which is a measure of the variability in the volume histogram analyses of the ADC values, showed a greater correlation with the fibrosis stage and inflammatory activity grade than did mean ADC, with a sensitivity of 0.91 and a specificity of 0.92 in the detection of inflammation.

In patients with chronic hepatitis C, a significant correlation between the pathologic fibrosis stage and the inflammatory activity grade is well known (36,37). Our results are consistent with those results and indicate that fibrosis tends to evolve as necroinflammation becomes more pronounced in chronic hepatitis C. Although the Spearman coefficient value was relatively low (r = 0.46), this trend may be one of the reasons why liver ADC showed an inverse correlation with both fibrosis stage and inflammatory activity grade. The possible biologic implications of a reduced mean ADC value and an increased entropy ADC value with increasing fibrosis stage and inflammation are intracellular alterations, changes of cellular composition, and decreased interstitial fluids according to the fibrosis stage and inflammatory activity grade.

Table 1

A_z Values for Mean and Entropy ADC according to METAVIR Fibrosis Score

Parameter	≥F1	≥F2	≥F3	F4
Mean ADC	0.889 (0.799, 0.978)	0.925 (0.851, 0.999)	0.926 (0.859, 0.993)	0.842 (0.730, 0.954)
Entropy ADC	0.937 (0.855, 1.0)	0.882 (0.787, 0.978)	0.855 (0.759, 0.950)	0.815 (0.675, 0.954)

Note.—Data are given as mean A_z values. Numbers in parentheses are 95% CIs. $P < .001$ for all comparisons.

Table 2

A_z Values for Mean and Entropy ADC according to METAVIR Activity Grade

Parameter	≥A1	≥A2	A3
Mean ADC	0.889 (0.799, 0.978)	0.807 (0.690, 0.925)	0.842 (0.722, 0.961)
Entropy ADC	0.937 (0.855, 1.0)	0.697 (0.554, 0.841)*	0.808 (0.691, 0.925)

Note.—Data are given as mean A_z values. Numbers in parentheses are 95% CIs. Except where indicated, $P < .001$.

* $P = .012$.

Our data highlight entropy ADC as a sensitive marker of overall hepatic damage that strongly correlated to pathologic fibrosis stage and inflammatory activity grade in patients with chronic hepatitis C. The most prominent finding of our study is the difference in entropy ADC values between patients without any signs of fibrosis (stage F0) and those with fibrosis of any pathologic stage (stages F1–F4) and between patients without inflammatory activity (grade A0) and those with any grade of inflammatory activity (grades A1–A3). Although other studies using entropy have not been performed in the abdomen, studies in patients with multiple sclerosis have shown that entropy can help measure macroscopic and microscopic tissue changes in the brain (25,26); neurologic damage has been reportedly associated with increased heterogeneity of signal intensities at DW imaging of the brain (25,26). As the distribution of these signal intensities becomes more heterogeneous (and the image therefore more random), entropy increases. Histopathologically, early fibrosis and inflammatory activity in chronic viral hepatitis demonstrate mild portal fibrosis and mild piecemeal necrosis and/or lobular necrosis (9,37) in addition to vascular changes (damage and disappearance of some branches of the portal veins) (38). In viral hepatitis, liver fibrosis begins in the portal triads and extends into the surrounding hepatic parenchyma. Thickening and lengthening of the fibrous septa results in the formation of fibrous bridges that link adjacent portal triads and central veins. With progressive liver injury, the bridges continue to enlarge and coalesce and eventually divide the liver into rounded islands of hepatic parenchyma (regenerative nodules) surrounded by fibrosis tissue. The change in tissue composition and architecture may be expected to increase barriers to water movement. The deposition of fibrous tissue leads to a reduction in the size or obliteration of small venules, with a resultant increase in portal venous pressure and consequent compensatory increased arterial blood flow. Changes in regional liver perfusion may have contributed to the increase in entropy ADC we observed in the early stages of liver disease. Infiltration of inflammatory cells into the liver interstitial tissue would also be expected to reduce water movement and increase liver ADC with regional variation. Regardless of early stage and grade, when these changes are combined, it causes the liver to go to a structure with an unstable architectural state according to chronic liver injury, from a normal structure with orderly normal tissue. The observation of increased liver entropy ADC depicted by means of the increased variability of ADC at

Table 3

Performance of Mean and Entropy ADC in the Prediction of METAVIR Fibrosis Score according to Cutoff Values

Parameter*	≥F1	≥F2	≥F3	F4
Cutoff mean ADC ($\times 10^{-3}$ mm²/sec)	1.35	1.32	1.27	1.23
Sensitivity	0.79 (0.64, 0.90)	0.85 (0.69, 0.95)	0.87 (0.66, 0.97)	0.75 (0.43, 0.95)
Specificity	0.83 (0.52, 0.98)	0.91 (0.70, 0.99)	0.84 (0.67, 0.95)	0.72 (0.56, 0.85)
PPV	0.94 (0.81, 0.99)	0.94 (0.79, 0.99)	0.80 (0.59, 0.93)	0.43 (0.22, 0.66)
NPV	0.53 (0.29, 0.76)	0.79 (0.58, 0.93)	0.90 (0.73, 0.98)	0.91 (0.76, 0.98)
Positive LR	4.7 (1.8, 16.7)	9.0 (3.2, 30.7)	5.6 (2.9, 9.4)	2.7 (1.4, 3.8)
Negative LR	0.25 (0.19, 0.47)	0.16 (0.11, 0.31)	0.15 (0.06, 0.36)	0.35 (0.12, 0.76)
Cutoff entropy ADC	1.30	1.43	1.48	1.58
Sensitivity	0.88 (0.72, 0.97)	0.82 (0.65, 0.93)	0.74 (0.52, 0.90)	0.67 (0.35, 0.090)
Specificity	0.92 (0.62, 0.99)	0.86 (0.64, 0.97)	0.78 (0.61, 0.89)	0.88 (0.75, 0.96)
PPV	0.97 (0.83, 0.995)	0.90 (0.74, 0.98)	0.71 (0.49, 0.87)	0.62 (0.31, 0.86)
NPV	0.69 (0.41, 0.89)	0.75 (0.53, 0.90)	0.81 (0.63, 0.93)	0.90 (0.77, 0.97)
Positive LR	10.6 (2.7, 58.8)	5.8 (2.5, 15.5)	3.4 (1.8, 6.1)	5.7 (2.4, 12.0)
Negative LR	0.13 (0.10, 0.25)	0.21 (0.13, 0.38)	0.33 (0.18, 0.61)	0.38 (0.18, 0.69)

Note.—Numbers in parentheses are 95% CIs.

* LR = likelihood ratio, NPV = negative predictive value, PPV = positive predictive value.

Table 4

Performance of Mean and Entropy ADC in the Prediction of METAVIR Inflammatory Activity Score according to Cutoff Values

Parameter*	≥A1	≥A2	A3
Cutoff mean ADC value ($\times 10^{-3}$ mm²/sec)	1.35	1.28	1.19
Sensitivity	0.81 (0.67, 0.92)	0.73 (0.54, 0.88)	0.77 (0.46, 0.95)
Specificity	0.83 (0.52, 0.98)	0.80 (0.59, 0.93)	0.83 (0.69, 0.93)
PPV	0.95 (0.82, 0.99)	0.81 (0.62, 0.94)	0.59 (0.33, 0.82)
NPV	0.56 (0.31, 0.78)	0.71 (0.51, 0.87)	0.92 (0.79, 0.98)
Positive LR	4.8 (1.8, 17.1)	3.7 (1.8, 7.9)	4.6 (2.3, 7.4)
Negative LR	0.22 (0.16, 0.43)	0.33 (0.21, 0.58)	0.28 (0.10, 0.60)
Cutoff entropy ADC value	1.30	1.43	1.51
Sensitivity	0.91 (0.78, 0.97)	0.73 (0.54, 0.88)	0.77 (0.46, 0.95)
Specificity	0.92 (0.62, 0.99)	0.60 (0.39, 0.79)	0.76 (0.61, 0.88)
PPV	0.98 (0.87, 0.99)	0.69 (0.50, 0.84)	0.50 (0.27, 0.73)
NPV	0.73 (0.45, 0.92)	0.65 (0.43, 0.84)	0.91 (0.77, 0.98)
Positive LR	10.9 (2.8, 59.7)	1.8 (1.1, 3.0)	3.2 (1.7, 4.7)
Negative LR	0.10 (0.08, 0.22)	0.44 (0.23, 0.84)	0.30 (0.11, 0.67)

Note.—Numbers in parentheses are 95% CIs.

* LR = likelihood ratio, NPV = negative predictive value, PPV = positive predictive value.

volumetric histogram analysis may therefore be a potential biomarker that reflects increased heterogeneity of hepatic parenchyma in diffuse liver disease. Furthermore, entropy ADC may be more helpful than mean ADC alone for detecting early stage fibrosis and early inflammatory activity.

There are a few limitations to our study. First, the study was retrospective and involved a small number of patients. A prospective study with a substantially larger sample is needed to further validate our findings. Second, because the pathologic specimens were obtained at surgery for a hepatic mass or with core biopsy, exact mapping of pathologic findings and imaging was not possible. However, our study was targeted at evaluating diffuse hepatic disease rather than characterizing focal lesions. Third, DW MR imaging is susceptible to motion artifacts that may interfere with quantitative measurements. We used respiratory-triggered DW MR imaging to reduce respiratory artifacts. The use of mean ADC and volumetric acquisition for entropy ADC should result in averaging of signal intensities to provide some compensation for respiratory motion. In addition, all measurements were obtained in the right lobe of the liver because the left lobe exhibits greater motion-related artifact. However, core liver biopsy, which is often used as the standard for staging the severity of liver disease, is also performed from the right lobe of the liver. Fourth, we used a combination of *b* values of 0 and 1000 sec/mm² for DW imaging. Further studies using a combination of at least three *b* values might be needed.

In summary, our data suggest that the diagnostic performance of mean or entropy ADC for predicting pathologic stage or inflammatory grade is at least similar to that of other DW MR imaging studies (22); however, the combination of mean and entropy ADC may improve diagnostic performances, particularly in the detection of inflammatory activity in the liver.

In practical clinical use, the evaluation with mean and entropy ADC may have several advantages: *(a)* The noninvasive nature of the examination allows for repeat performance; *(b)* entropy ADC may be able to help differentiate normal from any abnormal fibrosis stage or abnormal inflammatory activity grade and, thus, may represent indexes at the initiation of treatment and of improvement after treatment; and *(c)* mean ADC may reflect abnormal fibrosis stage (especially ≥F2 and ≥F3) and, thus, may help determine disease severity and the effects of therapy performed to treat hepatic fibrosis.

In conclusion, our preliminary data suggest that mean and entropy ADC might be helpful for predicting pathologic hepatic fibrosis stage and inflammatory activity grade in patients with chronic hepatitis C.

Disclosures of Potential Conflicts of Interest: K.F. Financial activities related to the present article: none to disclose. Financial activities not related to the present article: none to disclose. Other relationships: none to disclose. **T.T.** Financial activities related to the present article: none to disclose. Financial activities not related to the present article: none to disclose. Other relationships: none to disclose. **S.A.** Financial activities related to the present article: none to disclose. Financial activities not related to the present article: none to disclose. Other relationships: none to disclose. **M.K.** Financial activities related to the present article: none to disclose. Financial activities not related to the present article: none to disclose. Other relationships: none to disclose. **O.N.** Financial activities related to the present article: none to disclose. Financial activities not related to the present article: none to disclose. Other relationships: none to disclose. **T.J.** Financial activities related to the present article: none to disclose. Financial activities not related to the present article: none to disclose. Other relationships: none to disclose. **N.H.** Financial activities related to the present article: none to disclose. Financial activities not related to the present article: none to disclose. Other relationships: none to disclose. **K.O.** Financial activities related to the present article: none to disclose. Financial activities not related to the present article: none to disclose. Other relationships: none to disclose. **T.K.** Financial activities related to the present article: none to disclose. Financial activities not related to the present article: none to disclose. Other relationships: none to disclose. **M.S.** Financial activities related to the present article: none to disclose. Financial activities not related to the present article: none to disclose. Other relationships: none to disclose. **A.Q.** Financial activities related to the present article: none to disclose. Financial activities not related to the present article: none to disclose. Other relationships: none to disclose.

References

1. Ezelle HJ, Markovic D, Barber GN. Generation of hepatitis C virus-like particles by use of a recombinant vesicular stomatitis virus vector. J Virol 2002;76(23):12325–12334.
2. Afdhal NH. The natural history of hepatitis C. Semin Liver Dis 2004;24(suppl 2):3–8.
3. Strader DB, Wright T, Thomas DL, Seeff LB; American Association for the Study of Liver Diseases. Diagnosis, management, and treatment of hepatitis C. Hepatology 2004;39(4):1147–1171.
4. Tsukuma H, Hiyama T, Tanaka S, et al. Risk factors for hepatocellular carcinoma among patients with chronic liver disease. N Engl J Med 1993;328(25):1797–1801.
5. Hofmann WP, Zeuzem S, Hepatitis C. Hepatitis C: new therapeutic strategies needed for advanced disease. Nat Rev Gastroenterol Hepatol 2009;6(6):325–327.
6. Manning DS, Afdhal NH. Diagnosis and quantitation of fibrosis. Gastroenterology 2008;134(6):1670–1681.
7. Batts KP, Ludwig J. Chronic hepatitis: an update on terminology and reporting. Am J Surg Pathol 1995;19(12):1409–1417.
8. Knodell RG, Ishak KG, Black WC, et al. Formulation and application of a numerical scoring system for assessing histological activity in asymptomatic chronic active hepatitis. Hepatology 1981;1(5):431–435.
9. Ishak K, Baptista A, Bianchi L, et al. Histological grading and staging of chronic hepatitis. J Hepatol 1995;22(6):696–699.
10. Intraobserver and interobserver variations in liver biopsy interpretation in patients with chronic hepatitis C. The French METAVIR Cooperative Study Group. Hepatology 1994;20(1 pt 1):15–20.
11. Rozario R, Ramakrishna B. Histopathological study of chronic hepatitis B and C: a comparison of two scoring systems. J Hepatol 2003;38(2):223–229.
12. Talwalkar JA, Yin M, Fidler JL, Sanderson SO, Kamath PS, Ehman RL. Magnetic resonance imaging of hepatic fibrosis: emerging clinical applications. Hepatology 2008;47(1):332–342.
13. Mallet V, Gilgenkrantz H, Serpaggi J, et al. Brief communication: the relationship of regression of cirrhosis to outcome in chronic hepatitis C. Ann Intern Med 2008;149(6):399–403.
14. Friedrich-Rust M, Wunder K, Kriener S, et al. Liver fibrosis in viral hepatitis: noninvasive assessment with acoustic radiation force impulse imaging versus transient elastography. Radiology 2009;252(2):595–604.
15. Lewin M, Poujol-Robert A, Boëlle PY, et al. Diffusion-weighted magnetic resonance imaging for the assessment of fibrosis in chronic hepatitis C. Hepatology 2007;46(3):658–665.
16. Lucidarme O, Baleston F, Cadi M, et al. Noninvasive detection of liver fibrosis: is superparamagnetic iron oxide particle-enhanced MR imaging a contributive technique? Eur Radiol 2003;13(3):467–474.
17. Aguirre DA, Behling CA, Alpert E, Hassanein TI, Sirlin CB. Liver fibrosis: noninvasive diagnosis with double contrast material-enhanced MR imaging. Radiology 2006;239(2):425–437.
18. Koinuma M, Ohashi I, Hanafusa K, Shibuya H. Apparent diffusion coefficient measurements with diffusion-weighted magnetic resonance imaging for evaluation of hepatic fibrosis. J Magn Reson Imaging 2005;22(1):80–85.
19. Sandrasegaran K, Akisik FM, Lin C, et al. Value of diffusion-weighted MRI for assessing liver fibrosis and cirrhosis. AJR Am J Roentgenol 2009;193(6):1556–1560.
20. Taouli B, Tolia AJ, Losada M, et al. Diffusion-weighted MRI for quantification of liver fibrosis: preliminary experience. AJR Am J Roentgenol 2007;189(4):799–806.
21. Taouli B, Chouli M, Martin AJ, Qayyum A, Coakley FV, Vilgrain V. Chronic hepatitis: role of diffusion-weighted imaging and diffusion tensor imaging for the diagnosis of liver fibrosis and inflammation. J Magn Reson Imaging 2008;28(1):89–95.
22. Taouli B, Koh DM. Diffusion-weighted MR imaging of the liver. Radiology 2010;254(1):47–66.
23. Girometti R, Furlan A, Esposito G, et al. Relevance of *b*-values in evaluating liver fibrosis: a study in healthy and cirrhotic subjects using two single-shot spin-echo echo-planar diffusion-weighted sequences. J Magn Reson Imaging 2008;28(2):411–419.
24. Huwart L, Sempoux C, Vicaut E, et al. Magnetic resonance elastography for the noninvasive staging of liver fibrosis. Gastroenterology 2008;135(1):32–40.
25. Benedict RH, Bruce J, Dwyer MG, et al. Diffusion-weighted imaging predicts cognitive impairment in multiple sclerosis. Mult Scler 2007;13(6):722–730.
26. Tavazzi E, Dwyer MG, Weinstock-Guttman B, et al. Quantitative diffusion weighted imaging measures in patients with multiple sclerosis. Neuroimage 2007;36(3):746–754.
27. WMA Declaration of Helsinki—Ethical Principles for Medical Research Involving Human Subjects. Amended by the 59th WMA General Assembly, Seoul, October 2008. World Medical Association. http://www.wma.net/en/30publications/10policies/b3/index.html. Updated October 22, 2008. Accessed January 10, 2010.
28. Bland JM, Altman DG. Statistical methods for assessing agreement between two methods of clinical measurement. Lancet 1986;1(8476):307–310.
29. Ludbrook J. Statistical techniques for comparing measurers and methods of measurement: